AD NUMBER

AD822367

LIMITATION CHANGES

TO:

Approved for public release; distribution is unlimited. Document partially illegible.

FROM:

Distribution authorized to U.S. Gov't. agencies and their contractors; Critical Technology; SEP 1967. Other requests shall be referred to Air Force Technical Applications Center, Washington, DC 20330. Document partially illegible. This document contains export-controlled technical data.

AUTHORITY

usaf ltr, 25 jan 1972

TR67-54

TECHNICAL REPORT NO. 67-54

ANALYSIS OF TFSO LONG-PERIOD NOISE SURVEY DATA CONDUCTED UNDER PROJECT VT/7702

GEOTECH
A TELEDYNE COMPANY

TECHNICAL REPORT NO. 67-54

ANALYSIS OF TFSO LONG-PERIOD NOISE SURVEY DATA CONDUCTED UNDER PROJECT VT/7702

by

Dale S. Kelley

Sponsored by

Advanced Research Projects Agency
Nuclear Test Detection Office
ARPA Order No. 624

GEOTECH
A Teledyne Company
3401 Shiloh Road
Garland, Texas

18 September 1967

IDENTIFICATION

AFTAC Project No:	VELA T/7702
Project Title:	Operation of TFSO
ARPA Order No:	624
ARPA Program Code No:	
Name of Contractor:	Teledyne Industries Incorporated Geotech Division Garland, Texas
Date of Contract:	1 January 1967
Amount of Contract:	$1,090,300
Contract Number:	AF 33(657)-67-C-0091
Contract Expiration Date:	31 December 1967
Program Manager:	B. B. Leichliter, BR1-2561

CONTENTS

ILLUSTRATIONS

ILLUSTRATIONS, Continued

ILLUSTRATIONS, Continued

TABLES

ABSTRACT

The installation and checkout of a medium aperture long-period array at Tonto Forest Seismological Observatory is described. Methods of data selection and preparation for processing are given. Power spectra and phase velocities of the noise are computed; comparison with previously reported results show basic agreement. Coherence functions show peaks at the same frequencies in which the noise power is concentrated. In the frequency band 0.04 to 0.082 cps, the peak coherence is greater than 0.8 for station separations less than 10 kilometers. The coherence tends to decrease with increasing distance between stations.

ANALYSIS OF TFSO LONG-PERIOD NOISE SURVEY DATA CONDUCTED UNDER PROJECT VT/7702

1. INTRODUCTION

The basic purpose of seismometer arrays is to provide an output which gives signal enhancement through noise reduction. Designing arrays to achieve this goal can be approached in a logical and systematic way. The parameters of array design are seismometer pattern, number and spacing of seismometers, seismograph system response, and processing techniques. Proper control of these parameters utilizes the signal and noise properties to give an improved signal-to-noise ratio. The signal and noise properties of interest are wave number and frequency spectra, coherence, and dispersion functions. Detailed knowledge of these functions allow suitable choices of the array design parameters to be made. Thus it is evident that a knowledge of the signal and noise properties at the proposed site of an array is required.

2. SUMMARY OF PREVIOUS STUDIES AT THE TONTO FOREST SEISMOLOGICAL OBSERVATORY

The principal investigations of long-period noise characteristics at the Tonto Forest Seismological Observatory (TFSO) in the past were conducted by Texas Instruments (T. I.). Long-period data from a large aperture cross-linear array were recorded for T. I. in 1965. Their analysis of these data resulted in the following conclusions (T. I., 1966):

a. Teleseismic P-wave signals were coherent in the frequency band 0.04 to 0.09 cps over distances of at least 200 kilometers.

b. The power spectra of P-wave signals appeared to be space stationary for distances as large as 200 kilometers.

c. The recorded waveform of teleseismic body-wave signals had high visual correlation across the array.

d. The long-period noise exhibited no significant coherence at any frequency for seismometer separations of 50 kilometers or greater.

e. The noise power spectra on the vertical component showed strong similarity, though there was some variability in spectral level.

T. I. (1965) reported the phase velocity of 6-second Rayleigh waves at TFSO to be 3.4 kilometers per second, but a later report (T. I., 1967a) revised the estimate to 3.48 kilometers per second. T. I. (1967b) used data from a series of USGS calibration shots and two other explosions to construct a 5-layer crustal model for TFSO. A theoretical phase velocity dispersion curve for fundamental mode Rayleigh waves was computed from the model. The theoretical phase velocities varied from 3.8 to 3.2 kilometers per second in the frequency range 0.035 to 0.145 cps. A long-period event recorded at TFSO was time-partitioned and an experimental Rayleigh wave dispersion curve in the frequency range 0.025 to 0.175 cps was derived. Comparison of the theoretical and experimental curves showed good agreement.

The principal question left unanswered by previous long-period studies at TFSO is the following: What is the maximum separation between seismometers for which there is significant noise coherence? The aim of this study was to evaluate data from a medium aperture long-period array in an attempt to answer this question. A secondary objective was to obtain information regarding the noise spectra and phase velocities, providing a check of previous results.

3. GEOLOGY IN THE LONG-PERIOD ARRAY AREA

The portable system teams of the LRSM program were assigned to set up a medium aperture long-period array and to collect the data for this study. The LRSM teams collected data between 2 February and 7 April 1967. The general orientation and spacing of the portable system stations relative to TFSO and Payson, Arizona, is shown in figure 1. The legs of this "L" shaped array were located along azimuths of approximately 73 and 163 degrees. The approximate distance between adjacent stations was either 5 or 10 kilometers. Table 1 gives the coordinates and elevation of each station. The distance between all possible pairs of stations is given in table 2.

The geology of the array area is highly complex. A geologic cross section through Payson along an azimuth of 36 degrees is shown in figure 2. Igneous and metamorphic masses of Precambrian age underlie the entire array. To the south, these masses have been covered by Quaternary deposits of sand, silt, and gravel. To the north, they are overlain by sediments of Paleozoic age. The long-period array area has numerous faults. One major fault, with an east-west strike, occurs between TFSO and station PY4. Two other major faults are near station PY3, one west approximately 2.3 kilometers striking north-south and the other is to the north about 1.6 kilometers striking east-west.

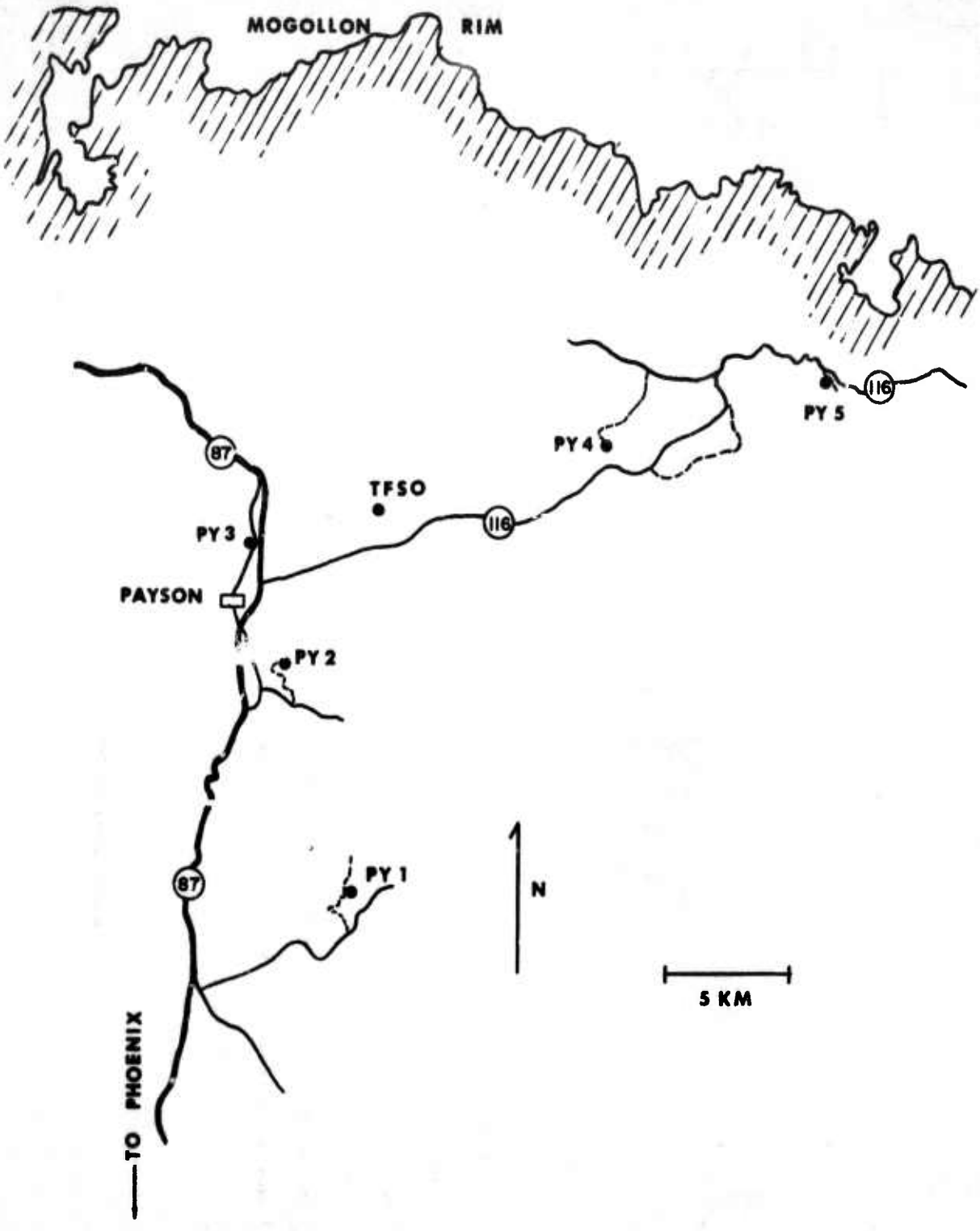

Figure 1. General orientation and spacing of the LRSM portable system stations relative to TFSO and Payson, Arizona

G 3142

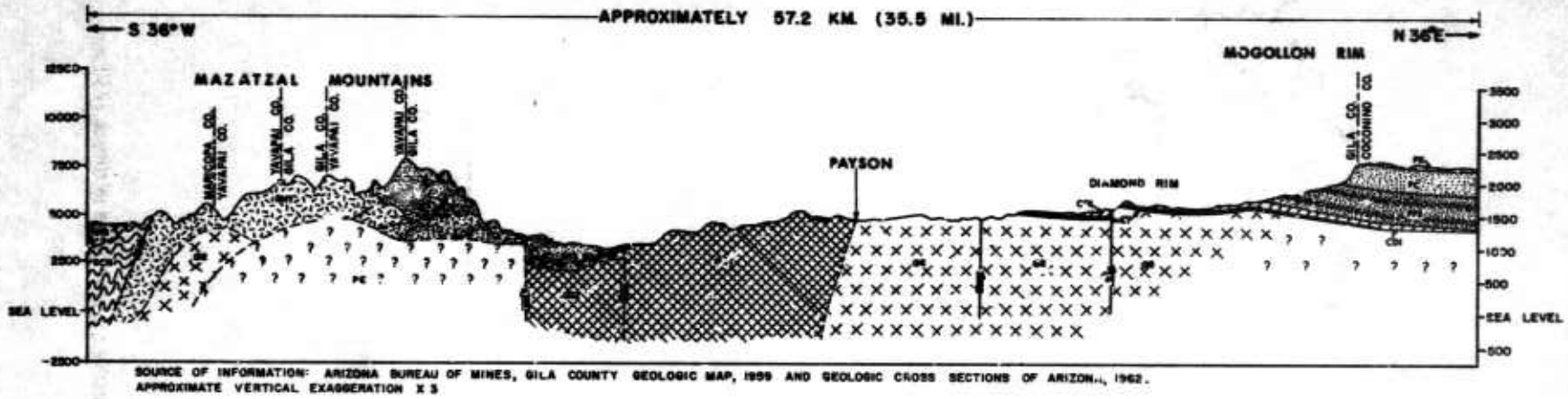

QTS	QUATERNARY, GRAVEL, SAND, AND SILT	GR	PRECAMBRIAN, GRANITE AND RELATED INTRUSIVE ROCKS
QTB	QUATERNARY, BASALT	MQ	PRECAMBRIAN, MAZATZAL QUARTZITE
PK	PERMIAN, KAIBAB LIMESTONE	SCH	PRECAMBRIAN, SCHIST
PC	PERMIAN, COCONINO SANDSTONE	RHY	PRECAMBRIAN, RHYOLITE
PPS	PERMIAN–PENNSYLVANIAN, SUPAI FORMATION, SANDSTONE & SHALE	GST	PRECAMBRIAN, GREENSTONE
CDI	PENN–MISS–DEVONIAN, LIMESTONE, SHALE, AND SANDSTONE	PC	PRECAMBRIAN, ROCK TYPE UNKNOWN
CT	CAMBRIAN, SANDSTONE AND QUARTZITE		

Figure 2. Generalized cross section through Payson, Arizona

G 3143

Topographically, the area is known as the Tonto Basin. The Mogollon Rim bounds the area on the north, with the Mazatzal Mountains to the west of the array area. To the south and east are the Sierra Ancha Mountains. The local topography of the array area is rough, with a total relief of 754 meters. The area is drained by the East Verde River to the west and Tonto Creek to the east of the array.

Table 1. Station coordinates and elevation

Station	Coordinates	Elevation
TFSO	34° 16' 04" N 111° 16' 13" W	1492 meters
PY1	34° 07' 36" N 111° 16' 52" W	1029 meters
PY2	34° 12' 40" N 111° 18' 45" W	1509 meters
PY3	34° 15' 15" N 111° 19' 37" W	1516 meters
PY4	34° 17' 34" N 111° 10' 00" W	1783 meters
PY5	34° 18' 58" N 111° 03' 47" W	1699 meters

Table 2. Distance between station pairs (kilometers)

PY1	15.8				
PY2	7.5	9.8			
PY3	5.4	14.8	5.0		
PY4	9.9	21.3	16.2	15.3	
PY5	19.8	29.1	25.7	25.2	9.9
	TFSO	PY1	PY2	PY3	PY4

4. PORTABLE SYSTEMS STATION INSTALLATION

The portable system stations were placed on the most competent rock available within 0.5 kilometer of the ideal location, and in areas with the least vegetation and cultural noise. All vault excavations were approximately 4 feet wide, 18 feet long, and were excavated to bedrock, which varied from 6 to 7 feet below the topsoil. Figure 3 shows the vaults in the excavation at PY3. Concrete pads 1.0 to 3.5 feet thick were poured on the bedrock. Pins were used to bond the concrete to the rock where necessary. The interiors of the tank vaults were sealed with epoxy and lined with fiberglass insulation before the seismometers were installed. The seismometers were covered with styrofoam

a. Vaults

b. Area in vicinity of PY3AZ

Figure 3. Long-period noise study vaults during installation and area in the immediate vicinity of PY3AZ

G 2653

and the remaining air space in the vault was filled with plastic bags of vermiculite. All lids were bolted to the vaults to ensure good seismometer insulation and vault pressure seal. The space between the vault and the excavation was backfilled with sawdust to ground level.

5. INSTRUMENTATION

Installation of the five portable systems began on 23 December 1966 and the stations became operational on 2 February 1967. Outputs from a set of three-component long-period seismographs were recorded at two levels on FM magnetic tape at each station. The outputs of the TFSO seismographs were also recorded on the Develocorder. Figures 4 and 5 show block diagrams of the seismograph systems at TFSO and the portable system stations. Check-out of the portable systems continued through February. In the checkout, close attention was paid to frequency and phase responses and system noise levels. At TFSO, the operating parameters of the seismograph system were modified so that the frequency and phase responses would match the portable system.

The system noise levels for the portable systems were checked by running dummy load tests in which the seismometer was replaced in the seismograph circuit by a resistor with the same value of resistance as the seismometer data coil. Figure 6 shows the relative levels of the system and seismic noise; the large deflections in this figure are caused by the removal of the resistor, and are neither system nor seismic noise. The system noise test data show that the system noise level is at least 18 dB below the level of the seismic noise. During routine recording of the data, extraneous noise was observed during windy periods. This noise was attributed in part to the effect of the wind blowing on the recording equipment package. In an effort to reduce these effects of wind, wooden covers were built and placed over the standard portable system shelter; however, the usefulness of these shelters in reducing the effects of wind noise was limited.

A mean phase response curve, shown in figure 7, was established from phase response measurements taken from the field recordings. Any system deviating from the mean by greater than 10 degrees at 18 seconds was brought into tolerance.

The amplitude responses of the portable long-period systems and the TFSO long-period systems were matched; a typical response is shown in figure 8.

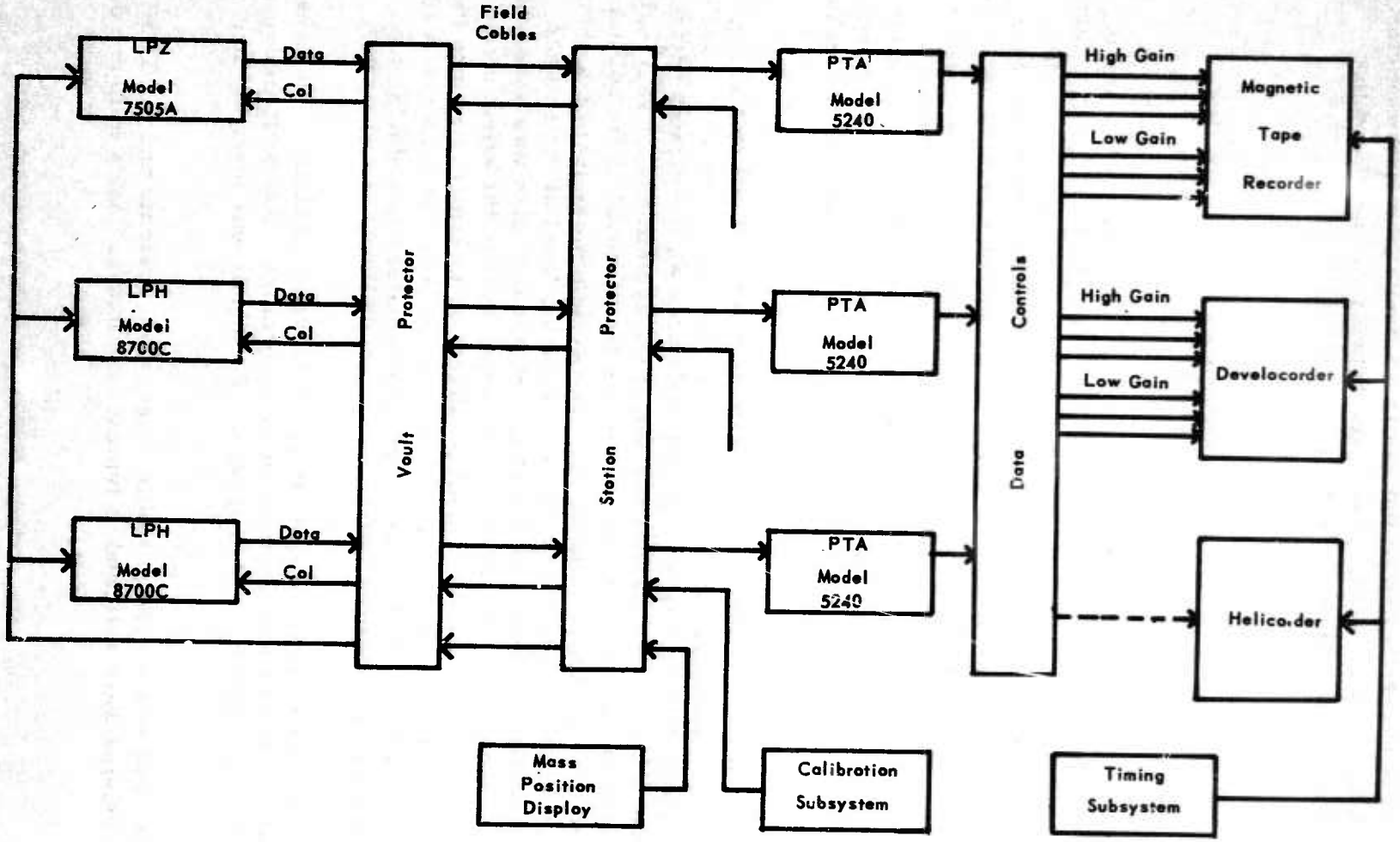

Figure 4. Block diagram of the TFSO long-period seismograph system

G 3144

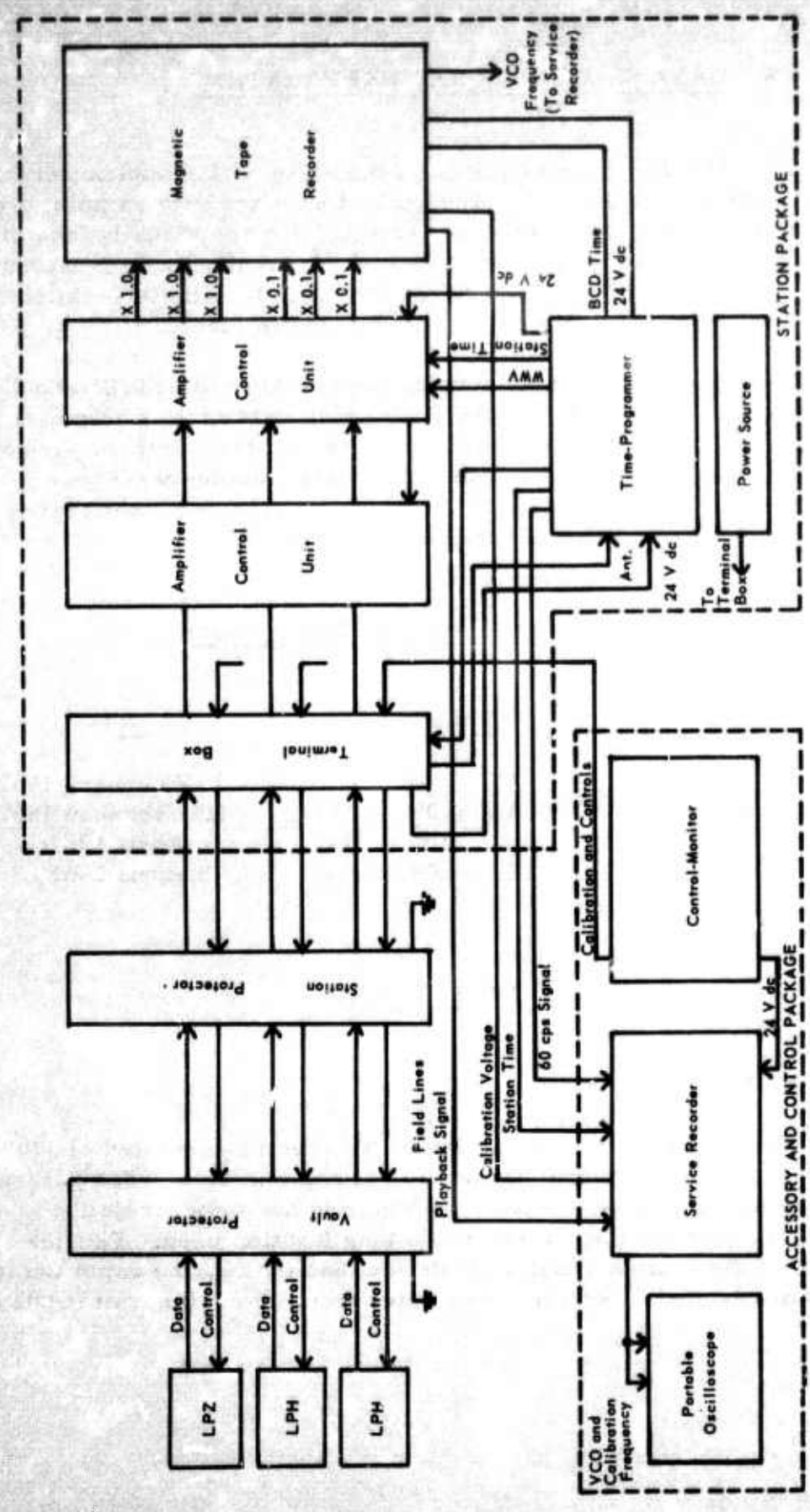

G 3145

Figure 5. Block diagram of the long-period portable seismograph system

6. DATA SELECTION AND PREPARATION

Thirty-five millimeter film transcriptions of the noise data samples were reviewed by an experienced analyst. The analyst selected data samples from the high-gain vertical-component seismograms which were visually free of nonseismic noise, and which showed evidence of the presence of 15-second microseisms. Table 3 gives the start times for the four samples selected for processing. Each of the samples was 40 minutes in length.

Before the data were digitized, they were band-pass filtered at 0.01 and 0.3 cps at rates of 18 dB per octave. Wow and flutter compensation was also used during playback. The data were sampled at the rate of two samples per second, giving a folding frequency of 1 cps. The digital data samples were gain equalized by using factors computed from a 0.04 cps sine-wave calibration most closely associated in time with the sample selected.

Table 3. Start times of selected data samples

Sample	Run	Time	Date
1	056	08:00:00	25 February 1967
2	056	18:00:00	25 February 1967
3	096	04:35:00	6 April 1967
4	095	13:45:00	5 April 1967

7. POWER SPECTRA

7.1 COMPUTATION

The digital samples used in the calculation of the spectra consisted of 3700 data points corresponding to about 31 minutes of seismic data. Ten percent lags and Parzen smoothing were used in calculating the autocorrelation functions. Figure 9 shows the Parzen smoothing function used. Fourier transformation of the smoothed autocorrelation functions by the rapid Cooley-Tukey algorithm resulted in spectral estimates from 0 to 1.0 cps at 0.002 cps increments.

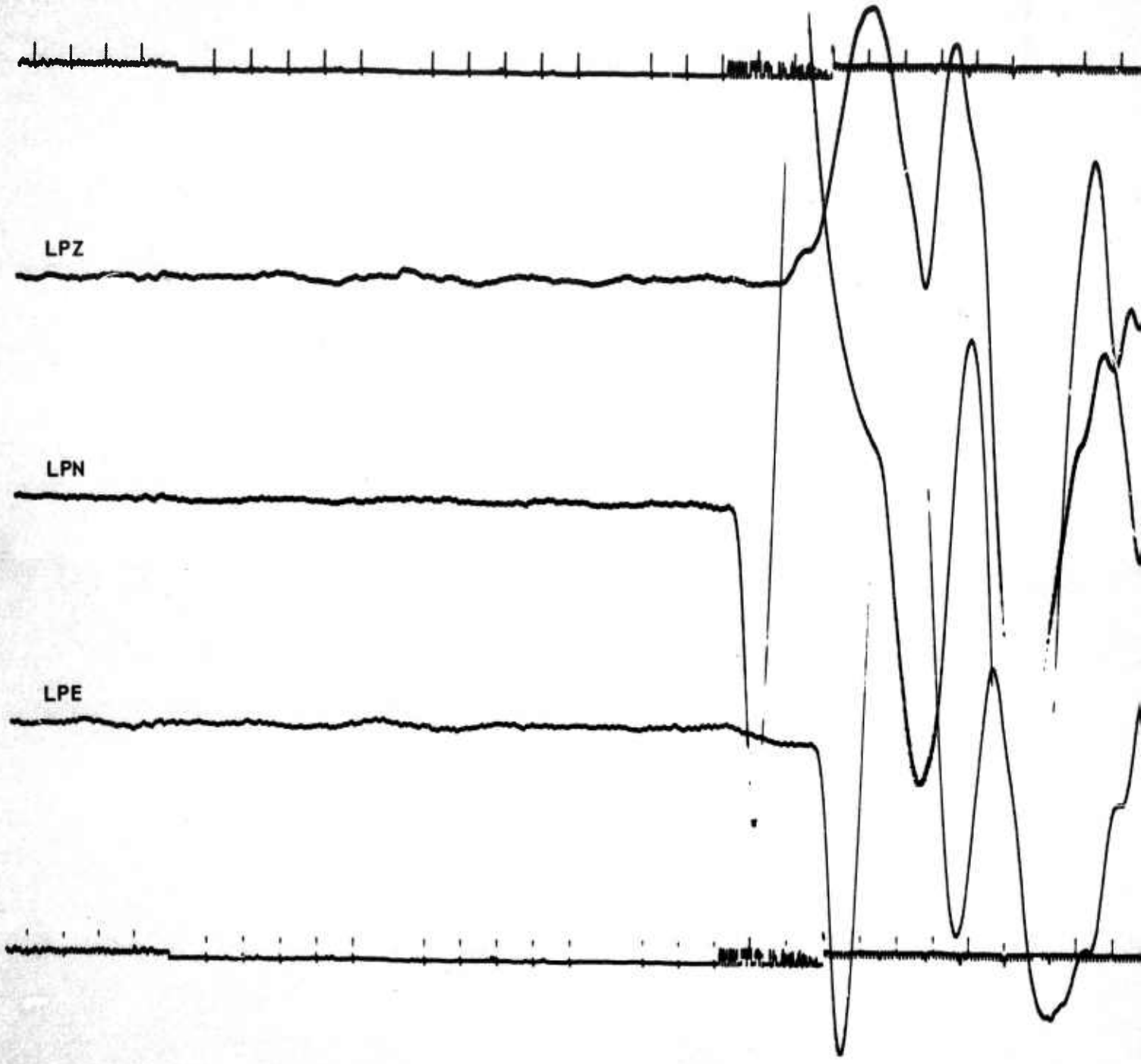
LPZ
LPN
LPE

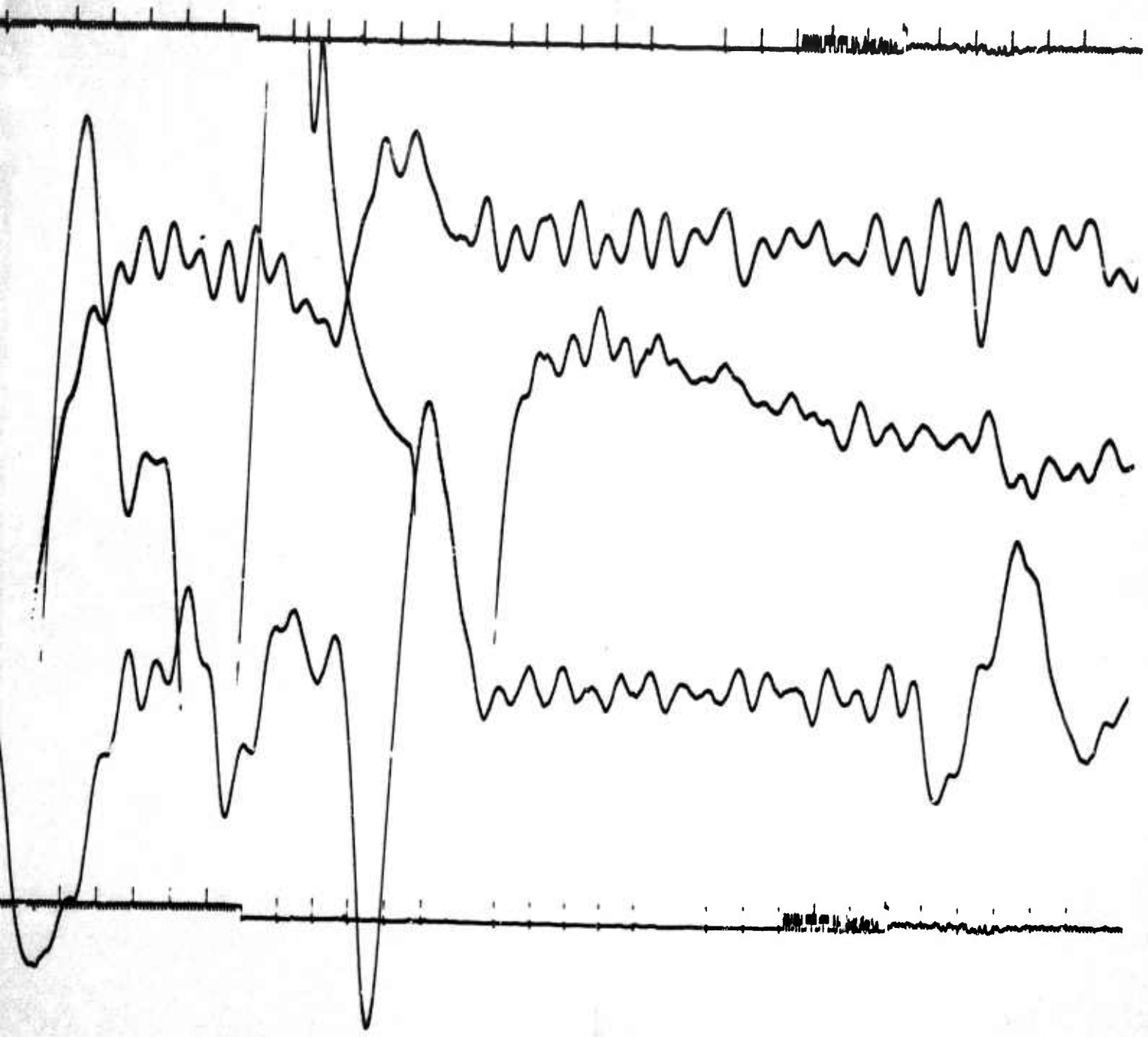

Figure 6. Seismogram showing the relative level of the system and seismic noise. The large deflections are caused by the removal of a resistor from the circuits

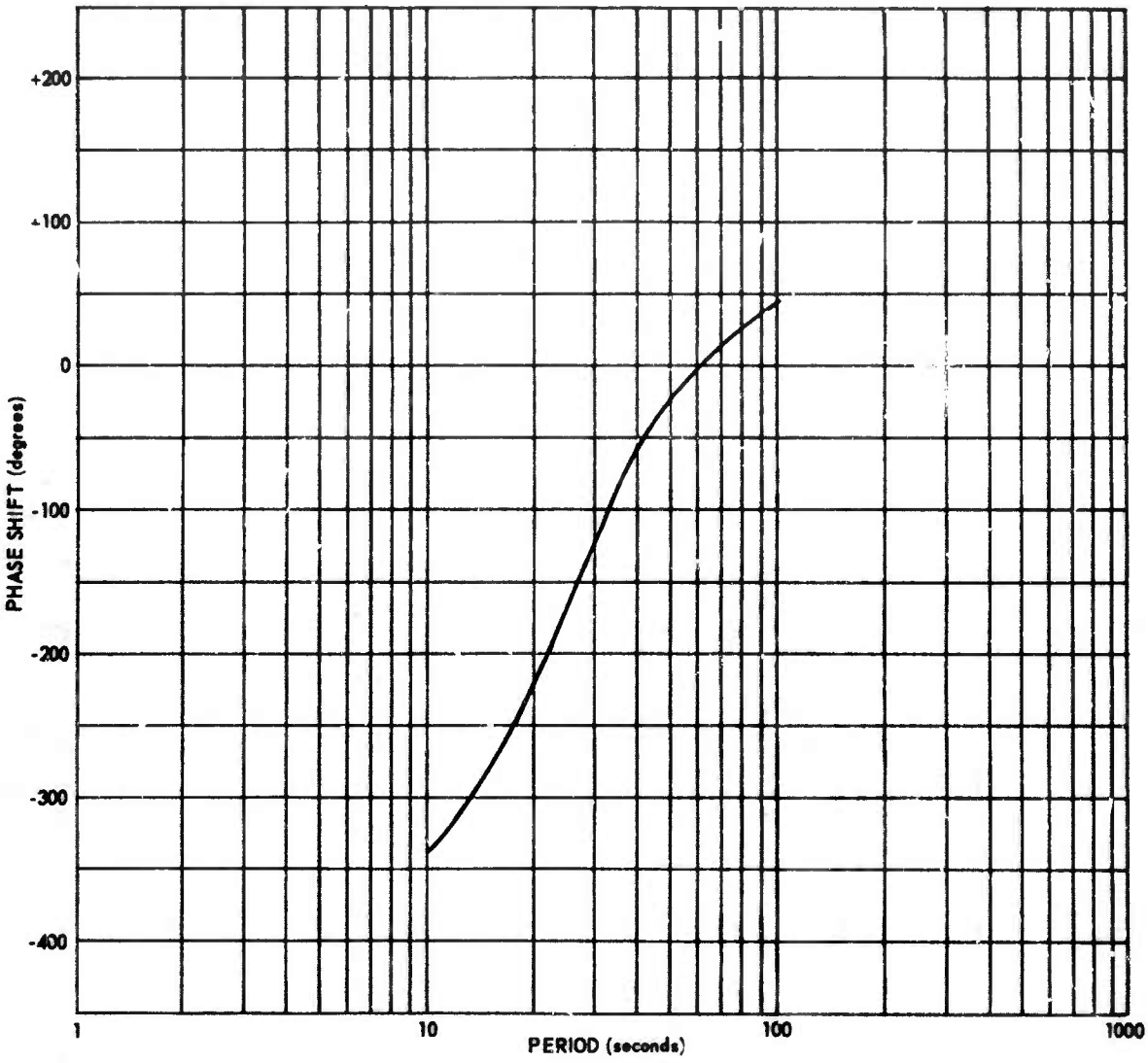

Figure 7. Average phase response for long-period systems

G 2654

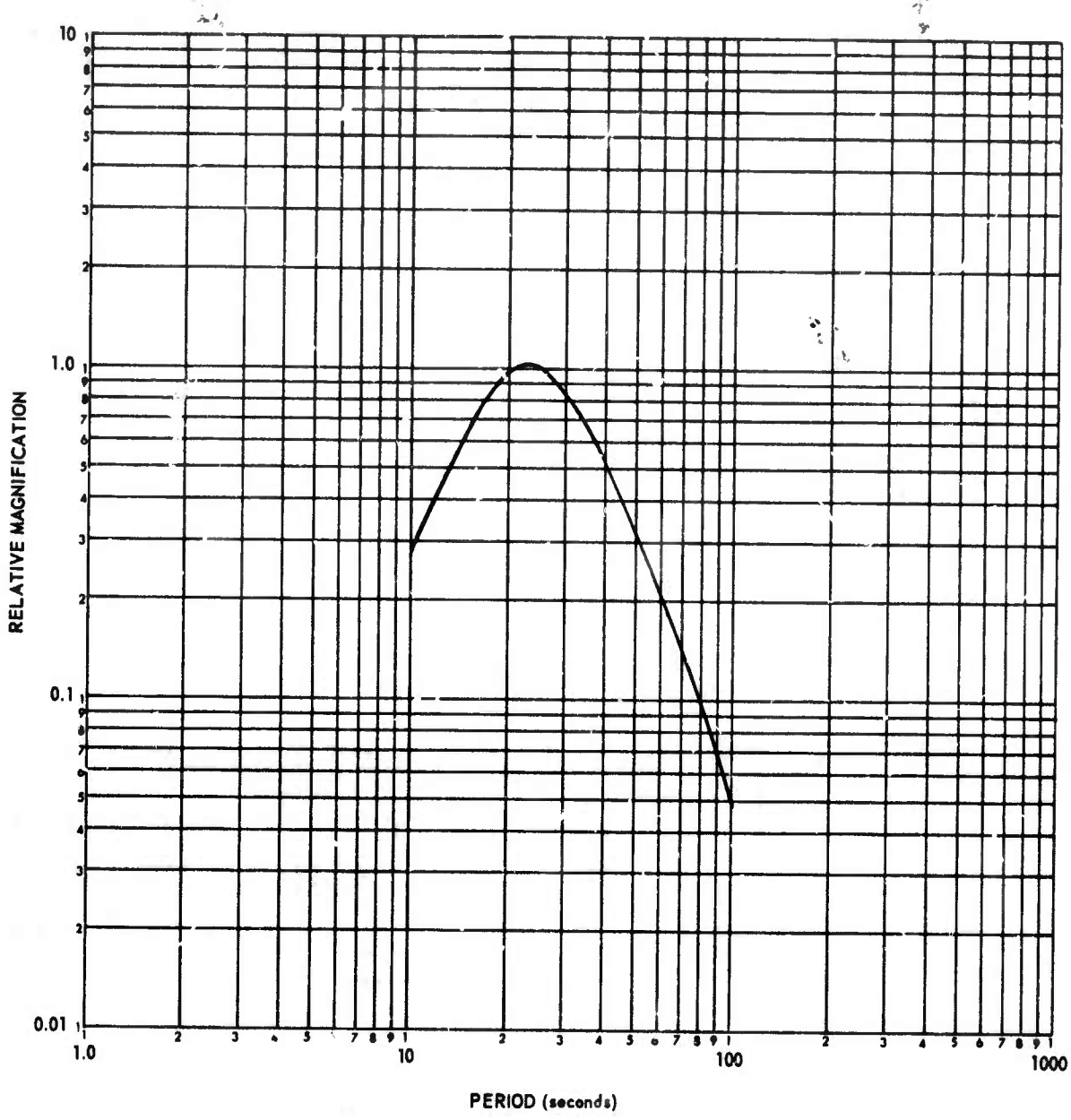

Figure 8. Typical amplitude response for portable system and TFSO long-period systems

G 2642

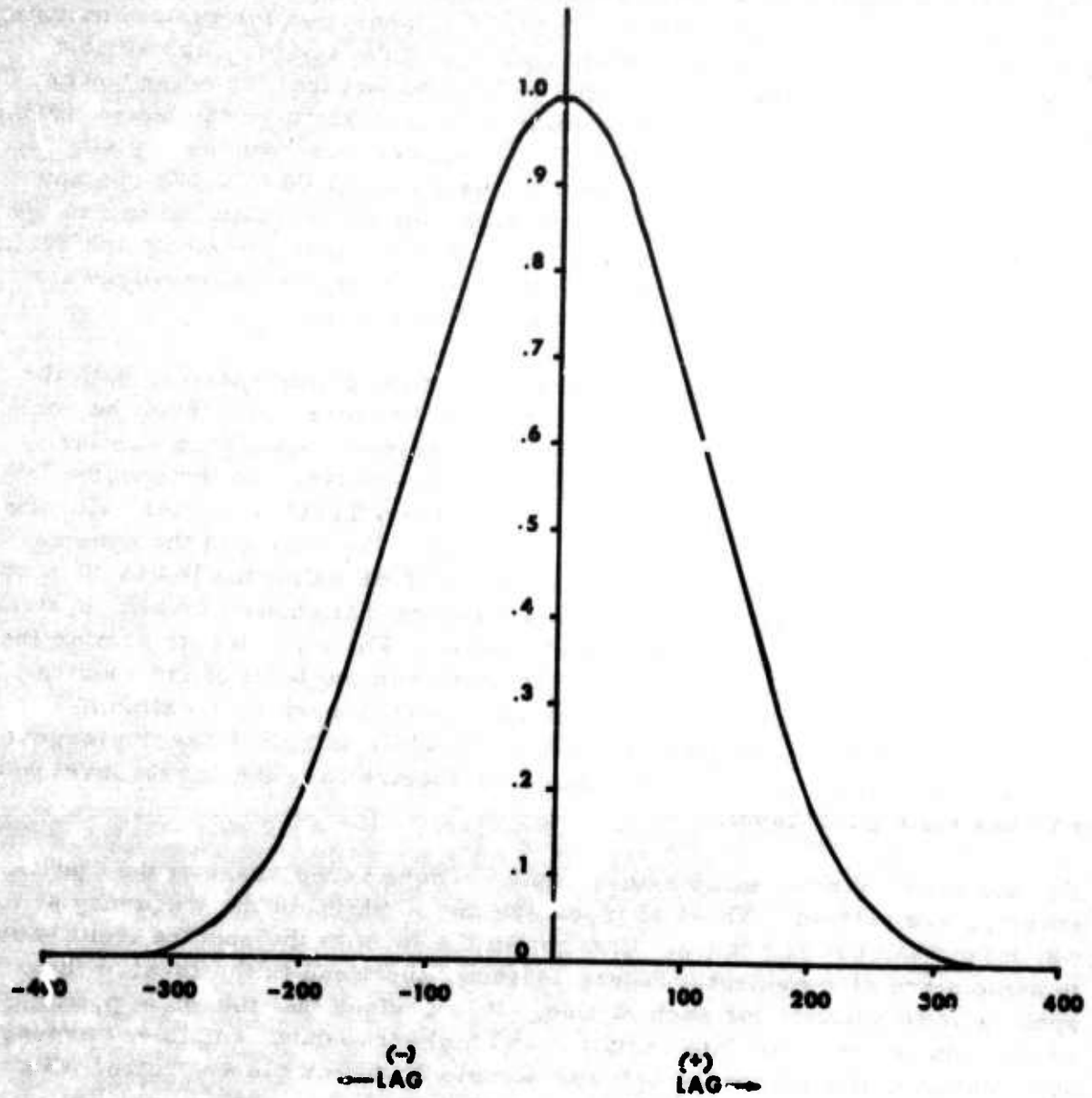

Figure 9. Parzen smoothing function applied to correlation functions

G 3146

7.2 RESULTS

Figures 10 through 13 show power spectra in the frequency range 0.025 to 0.165 cps for the four noise data samples. Compensation for system magnifications at 0.04 cps was made, but the effects of the seismograph system amplitude-response have not been removed. The fact that the noise power occurs in two frequency bands is a common characteristic of the power spectra for seismic noise in this pass band. The ranges of these bands vary slightly from sample to sample, but in general the bands are 0.04 to 0.082 cps and 0.11 to 0.165 cps. Within each of these bands the peak usually occurs in the intervals 0.05 to 0.063 cps and 0.125 to 0.145 cps. If the seismograph system amplitude response was removed from the spectra, the actual earth motion spectral peaks would shift to slightly higher frequencies.

In evaluating the degree of space stationarity of the power spectra, both the shape of the spectral envelope and the level of the noise power must be considered. For each data sample, the power spectrum shows good similarity in the main features of the envelope. This high similarity of the spectra from the portable system stations with the spectra from TFSO is further evidence that the data recorded were true seismic noise. The trough in the spectra between 0.091 and 0.10 cps is generally 15 to 20 dB below the 16- to 20-second peak, supporting the data from dummy load tests that showed that the system noise was about 18 dB below the seismic noise. For a given data sample there is considerable variation from station to station in the level of the spectra. Sample 4 has the smallest station-to-station variation with a maximum variation between two stations of about 3 dB, while sample 3 has the largest variation with about 12 dB. TFSO and PY2 spectra have the lowest level while PY3 has the highest level.

For the same station, sample-to-sample changes in the shape of the spectral envelope are evident. These changes are due to shifts in the frequency at which the peak power occurs. Changes in the level of the spectra from sample to sample are also evident. Figure 14 shows the trend in the level of the spectra at 16 seconds for each station. It is obvious that the noise power at 16 seconds is lowest in data sample 2 and highest in data sample 4. Averaging over stations, the difference between sample 2 and sample 4 spectral levels is about 9 dB at 16 seconds.

7.3 CONCLUSIONS

The power spectra possess the following characteristics:

a. The noise power is concentrated in two frequency bands, 0.04 to 0.082 cps and 0.11 to 0.165 cps.

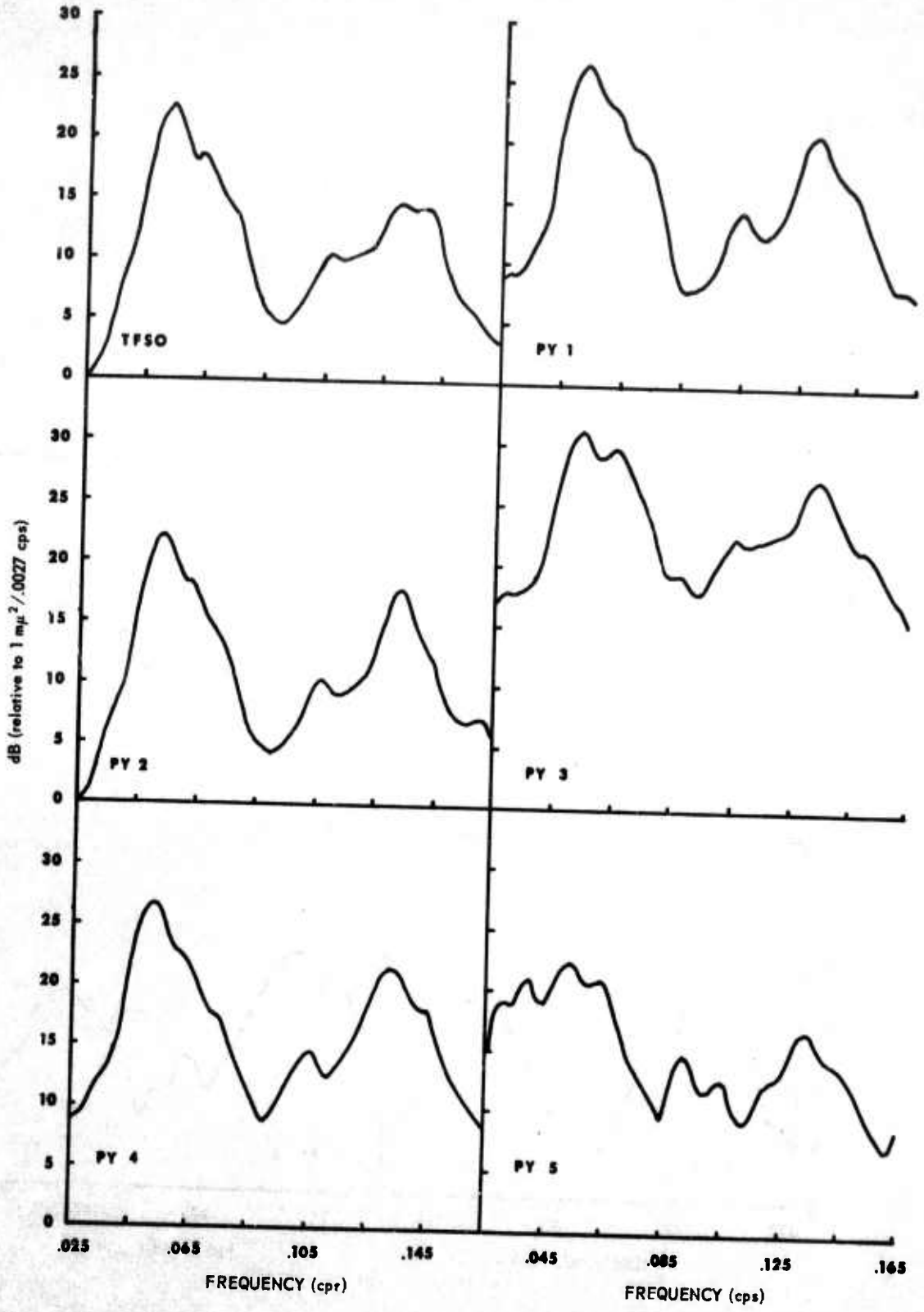

Figure 10. Power spectra for each station for first data sample

G 3147

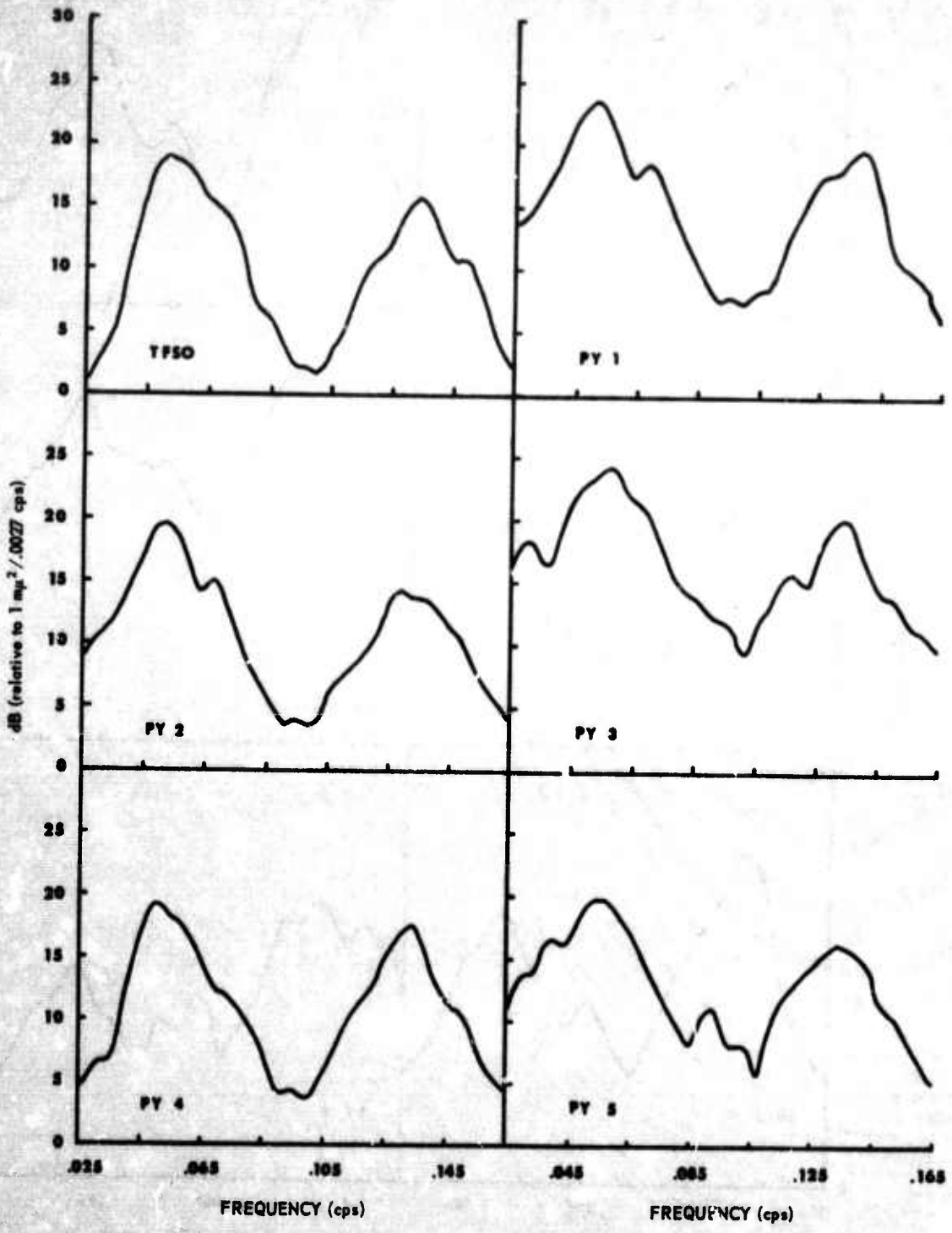

Figure 11. Power spectra for each station for second data sample

G 3143

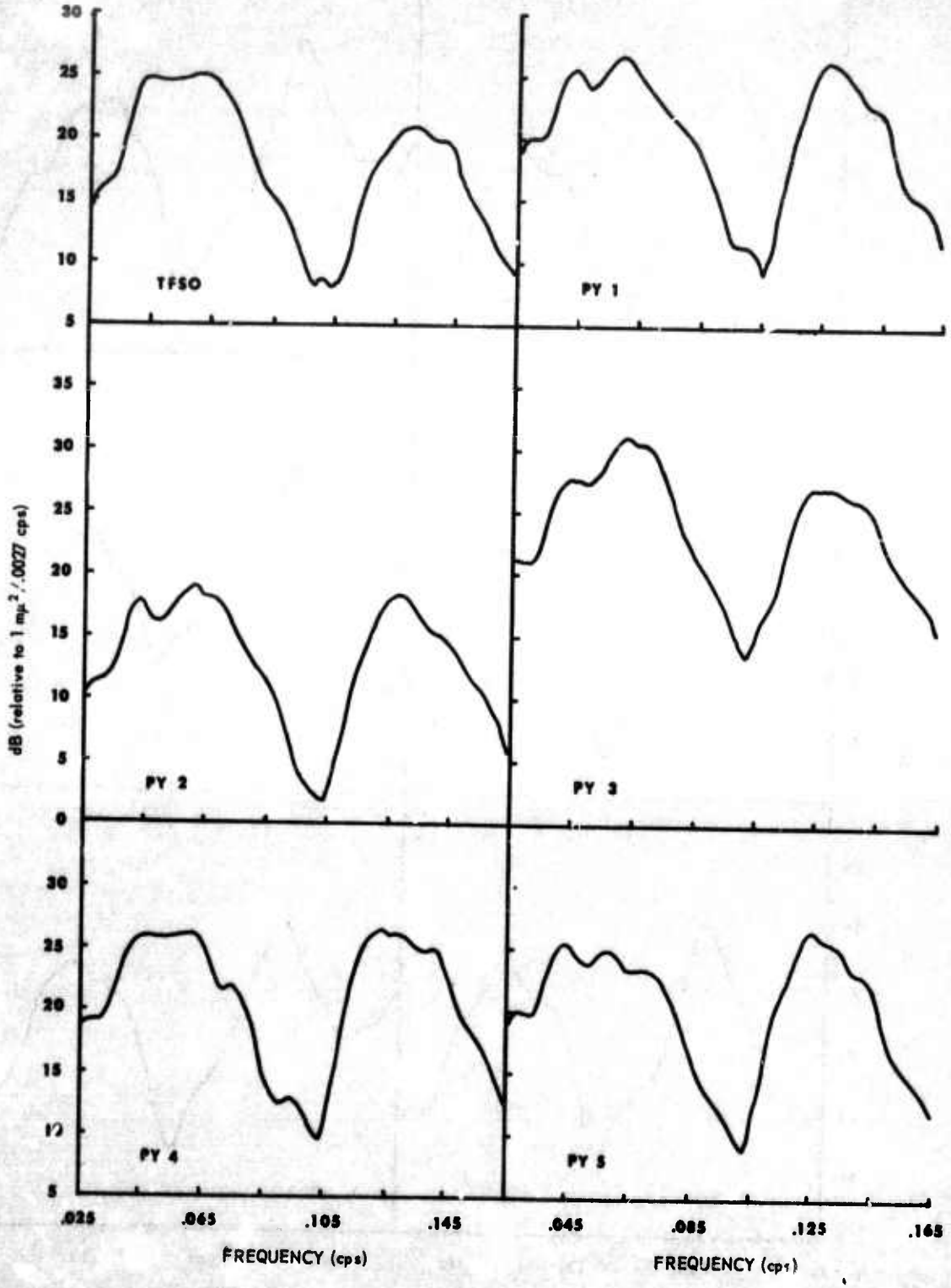

Figure 12. Power spectra for each station for third data sample

G 3149

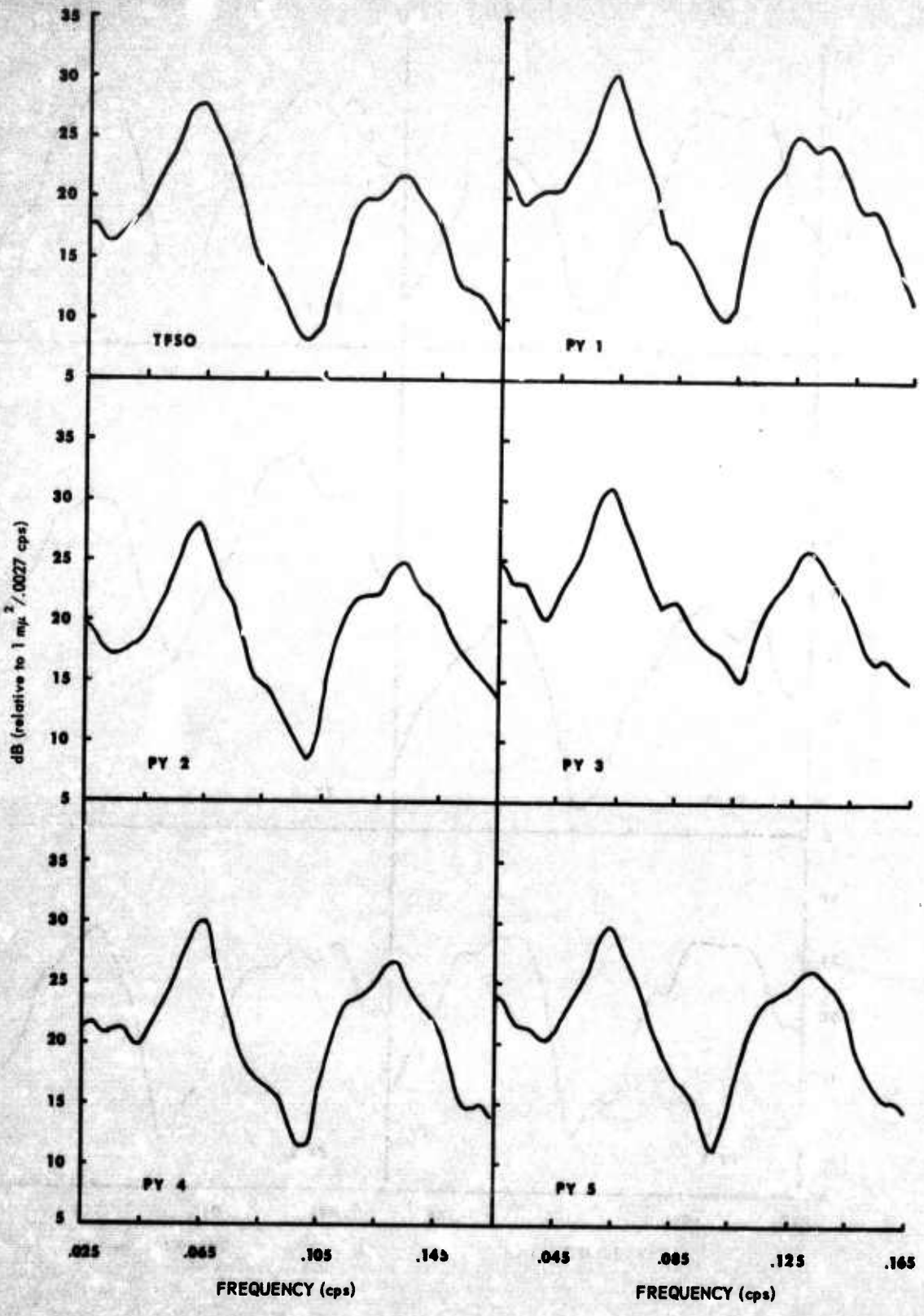

Figure 13. Power spectra for each station for fourth data sample

G 3150

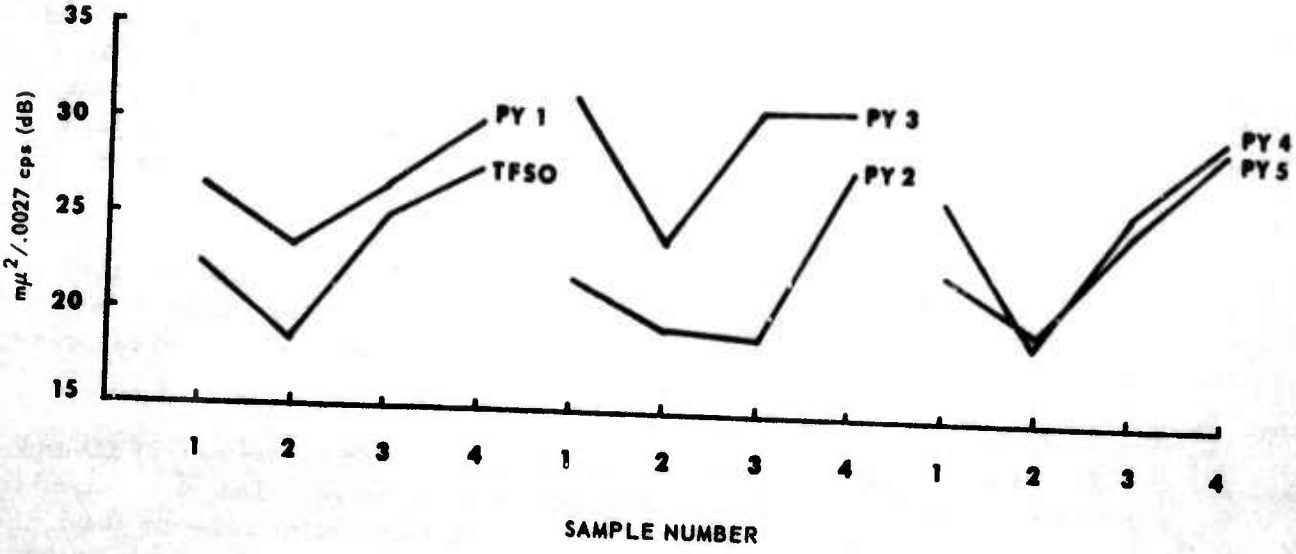

Figure 14. Relative spectral level at 16 seconds for four data samples

b. The power spectra may be space stationary but relative variations in spectral level cause some doubt.

c. The power spectra are not time stationary.

It should be noted that these characteristics are in good agreement with the characteristics of the noise power spectra for data samples from the extended cross-linear long-period array (T. I., 1966).

8. PHASE VELOCITY

The basic approach to measuring phase velocity of the noise was the standard method of determining relative time delays across a tripartite array. The time delays and the tripartite geometry give apparent velocity vectors from which azimuth of propagation and phase velocity are computed. The validity of this method depends on the accuracy of the assumption that the noise is unidirectional.

The time delays across the tripartite were measured from the phase angles associated with the cross-power spectra. The reliability of the time delays obtained in this manner is reasonably good, since frequencies of interest were determined by high coherence and large noise power.

Figure 15 shows the theoretical phase velocity dispersion curve for TFSO and the experimental phase velocities measured from the noise. The experimental points show some scatter; however, there is basic agreement between the theoretical and experimental phase velocities. The scatter in the experimental data is probably due to the presence of multiple noise sources, measurement error in the phase angles, and slight differences in the system phase responses.

9. COHERENCE

9.1 COMPUTATION

The cross-power spectra were computed in the same way as the auto-power spectra discussed in section 7.1 were computed. Letting $S_{ij}(f)$ denote the power spectrum ($i = j$, auto; $i \neq j$, cross) for stations i and j, coherence was computed by the formula $C_{ij}(f) = \frac{|S_{ij}(f)|}{\sqrt{S_{ii}(f) \cdot S_{jj}(f)}}$. For an ensemble of weakly stationary bivariate Gaussian processes, the probability distribution of the

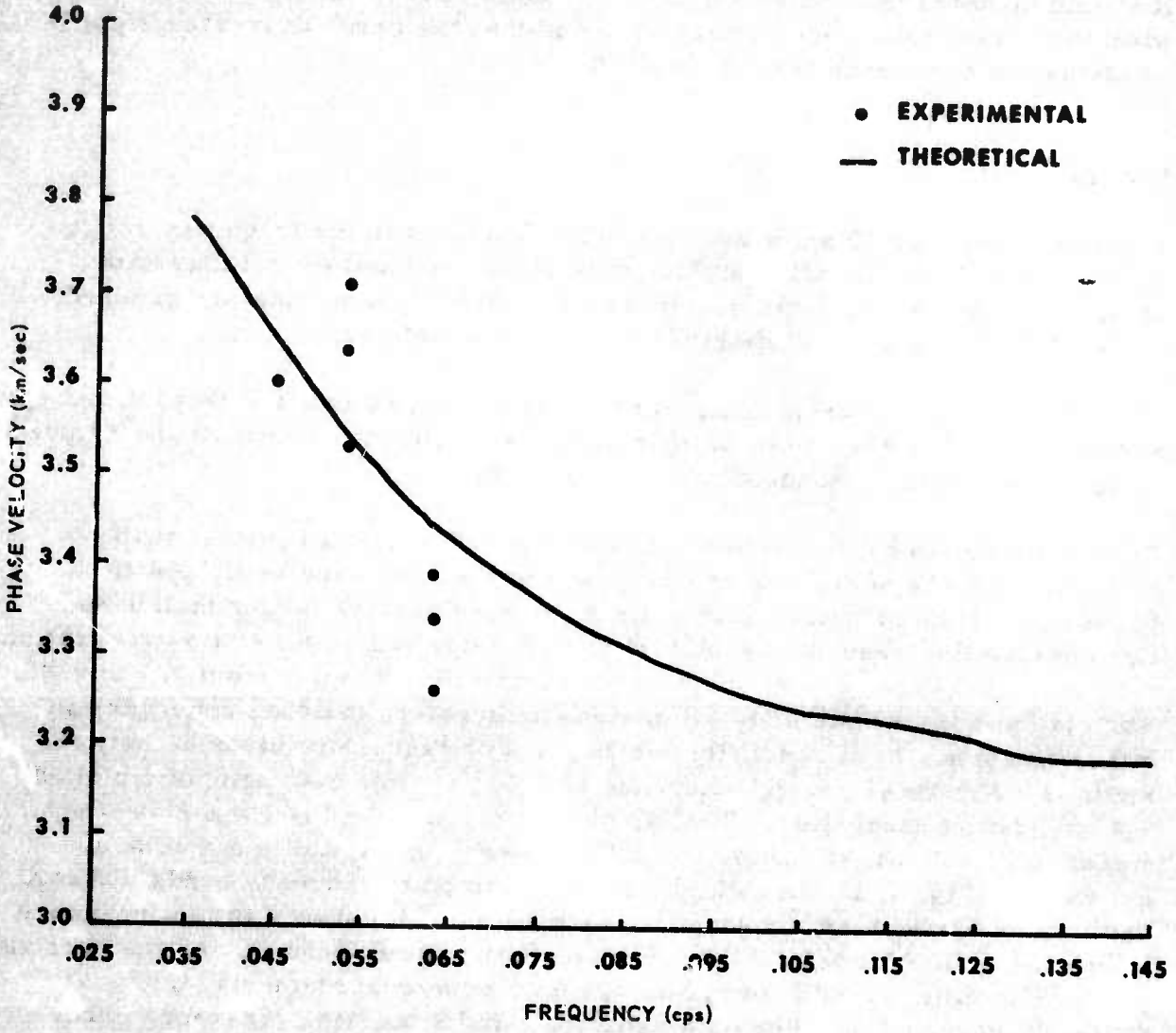

Figure 15. Theoretical and experimental phase velocities

G 3152

coherence coefficients for all possible pairs has been determined (Amos, et al., 1963). Experimental coherence functions depend on the actual coherence, the smoothing function, and the lag window. For Parzen smoothing and 10 percent lags, the 90 percent confidence limits are shown in figure 16. It should be noted that considerable error can occur in the measured coherence when the actual coherence is near zero and that the error decreases significantly as the coherence approaches 1.0.

9.2 RESULTS

Figures 17 through 40 show the coherence functions in the frequency range 0.025 to 0.165 cps for all possible pairs of stations and for all four data samples. The 15 coherence functions for a given data sample are grouped arbitrarily on the basis of distance between the stations.

The values of the coherence functions in the frequency bands 0.04 to 0.082 cps and 0.11 to 0.165 cps are of primary interest because between 70 and 80 percent of the noise power is concentrated in these two bands.

Coherence functions for station pairs with small separations (less than 10 kilometers) have high coherence peaks in the frequency band 0.04 to 0.082 cps. Nine of twelve such coherence functions are larger than 0.80. Considering the frequency band 0.11 to 0.165 cps and small station separations, the peak coherence shows considerable variability, ranging from 0.4 to 0.85. For station separations of 10 kilometers or greater, the peak coherence in either frequency band generally decreases with increasing distance between stations. Figure 41 shows coherence at 0.043 cps for data sample 3 plotted against station separation. Similar plots for data samples 1 and 2 at other frequencies indicate the same trend. However, this trend is not without exception. Figure 40 shows high coherence in both frequency bands although the station separations are large. The maximum coherence in the frequency band 0.04 to 0.082 cps usually occurs near the same frequency as the spectral peak. For different data samples, the maximum coherence may occur at different frequencies. For data samples 1 and 2 the peak coherence occurs about 0.05 cps, while the coherence for data samples 3 and 4 peak about 0.065 cps. This shifting of peak coherence contributes to the absence of time-stationarity.

The data for evaluating space stationarity of the coherence functions are limited since (TFSO, PY4) and (PY4, PY5) is the only repetition of vector pairs. However, data from these pairs indicate that the coherence functions depend on actual station location.

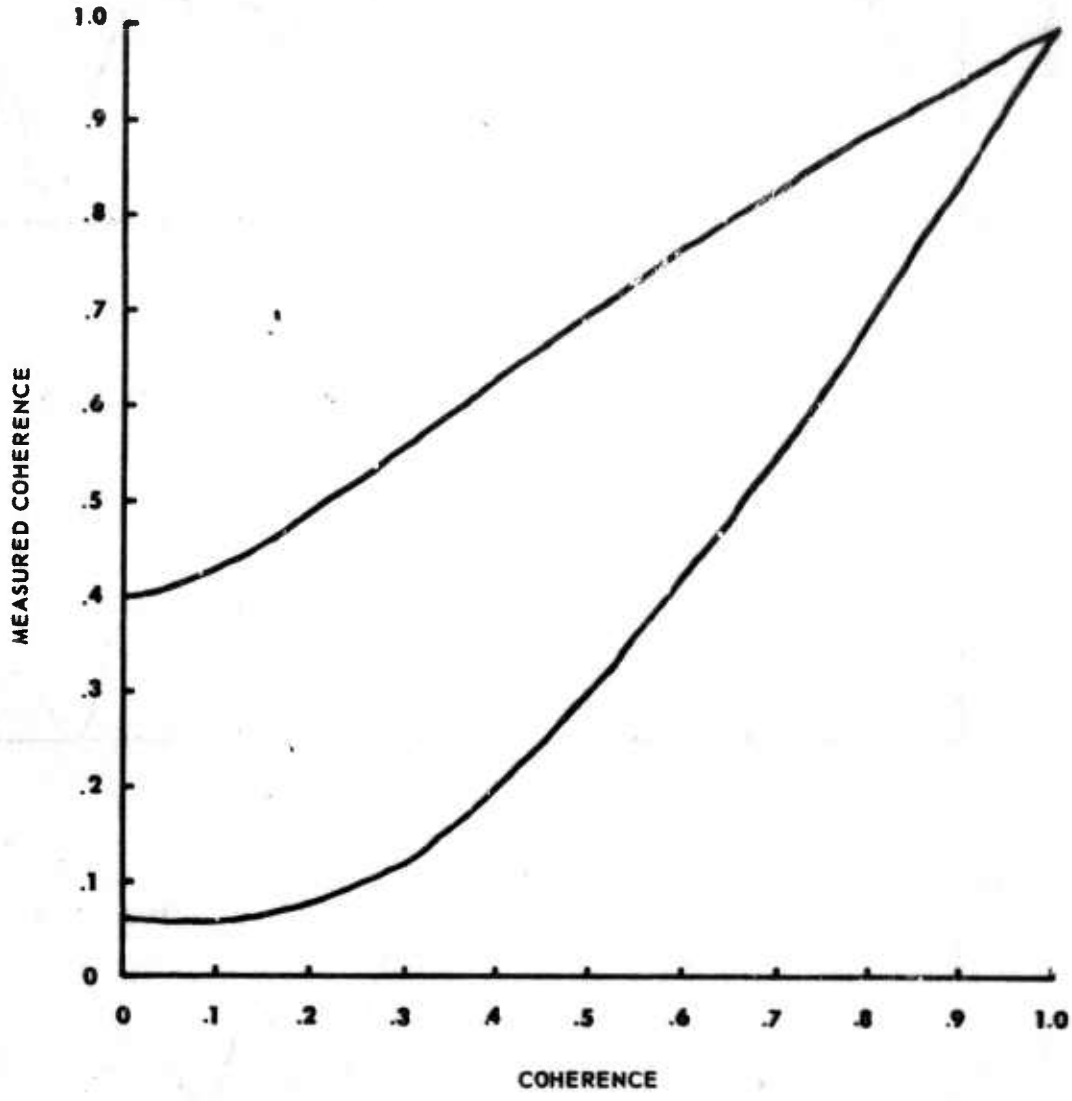

Figure 16. Ninety percent confidence limits for measured coherence

G 3153

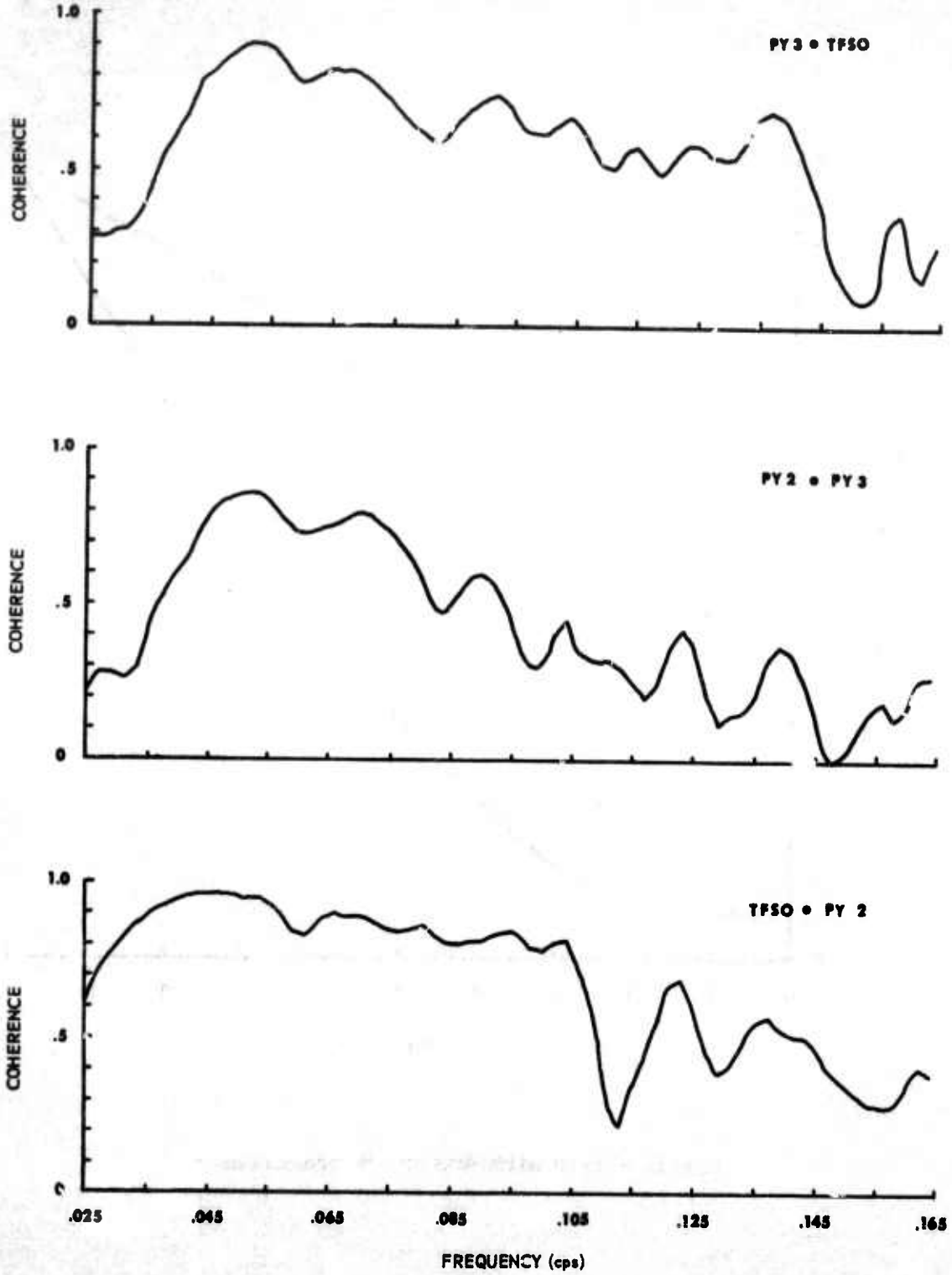

Figure 17. Coherence functions for data sample 1 for station separations less than 10 kilometers

G 3154

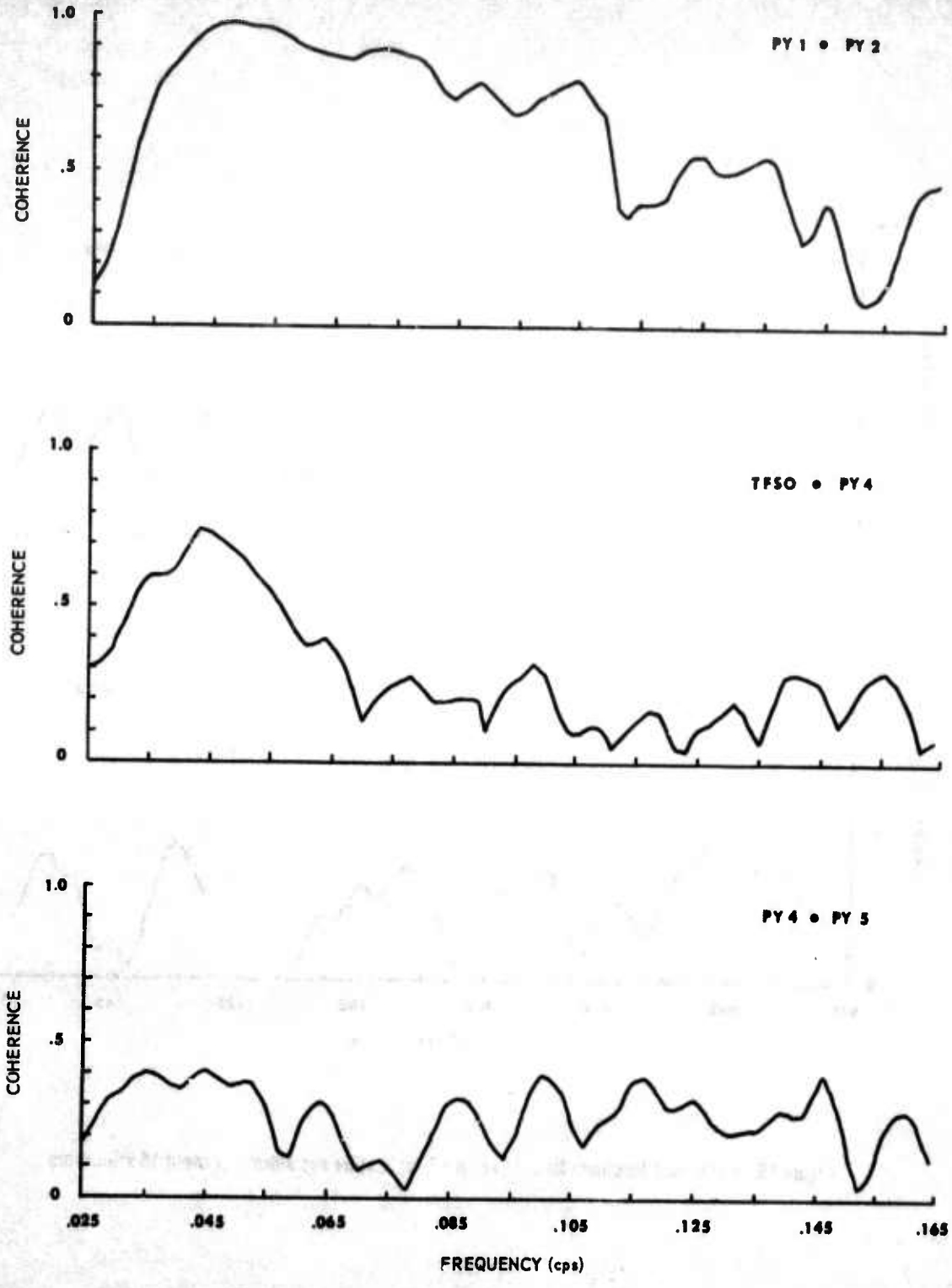

Figure 18. Coherence functions for data sample 1 for station separations of about 10 kilometers

G 3155

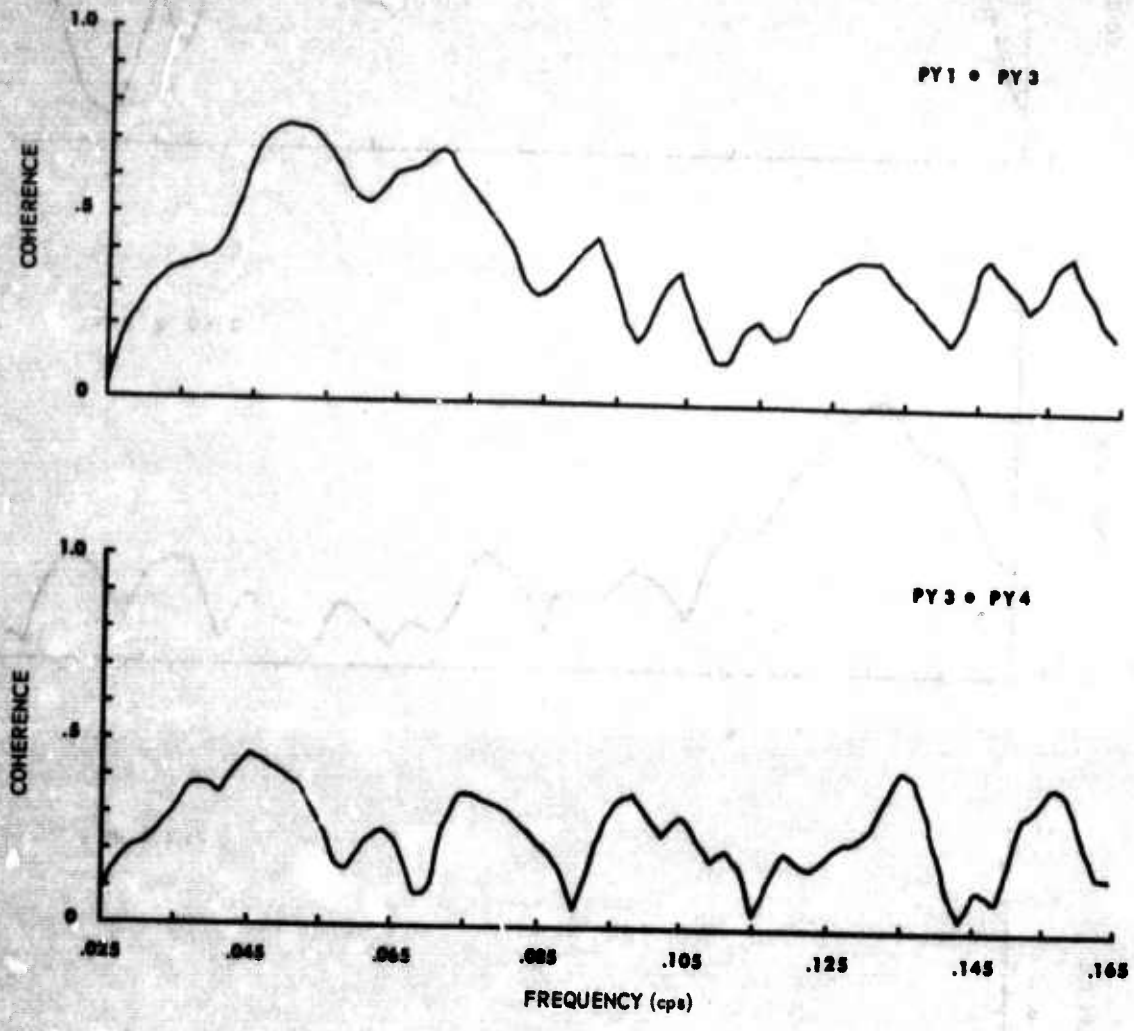

Figure 19. Coherence functions for data sample 1 for station separations of about 15 kilometers

G 3156

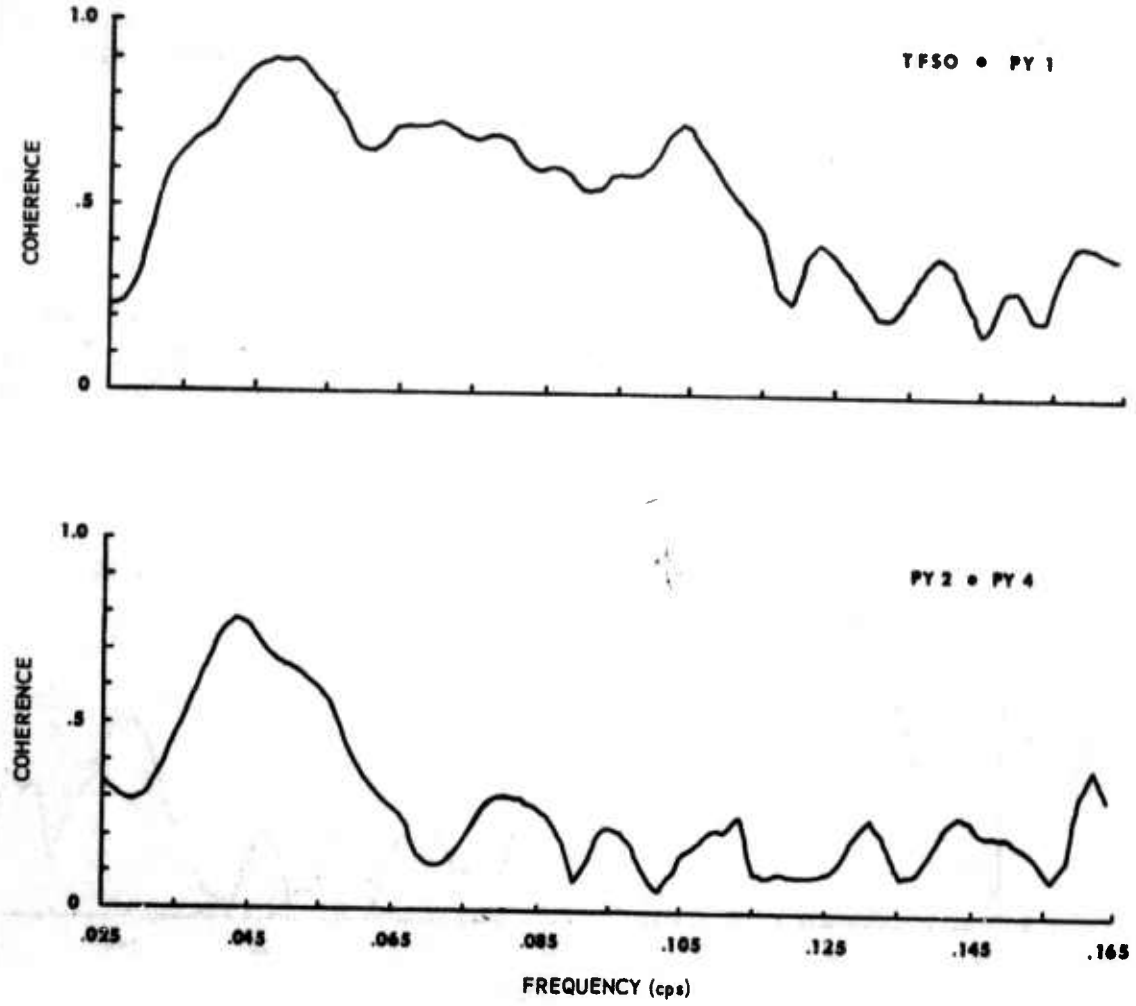

Figure 20. Coherence functions for data sample 1 for station separations of about 15.8 kilometers

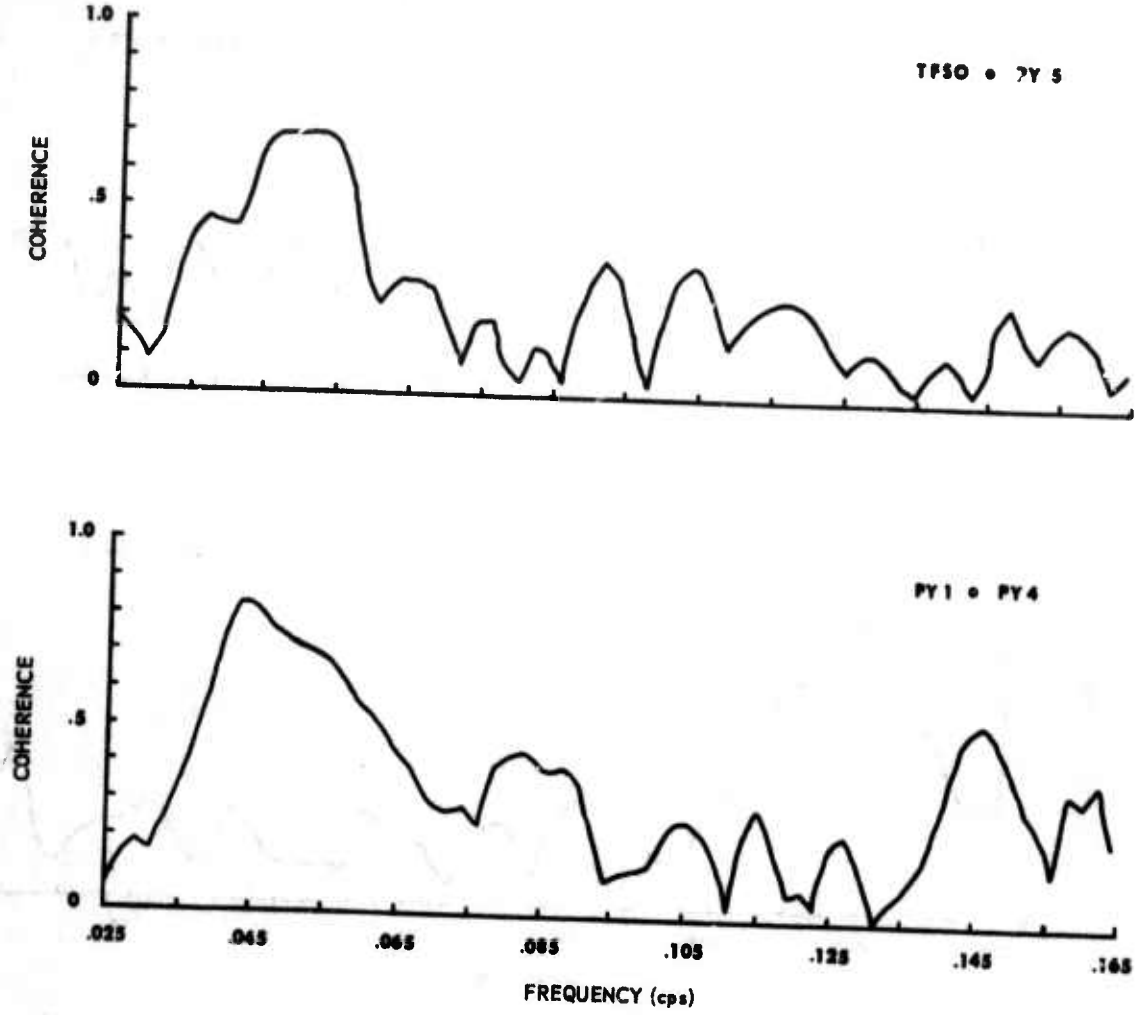

Figure 21. Coherence functions for data sample 1 for station separations of about 20 kilometers

G 3158

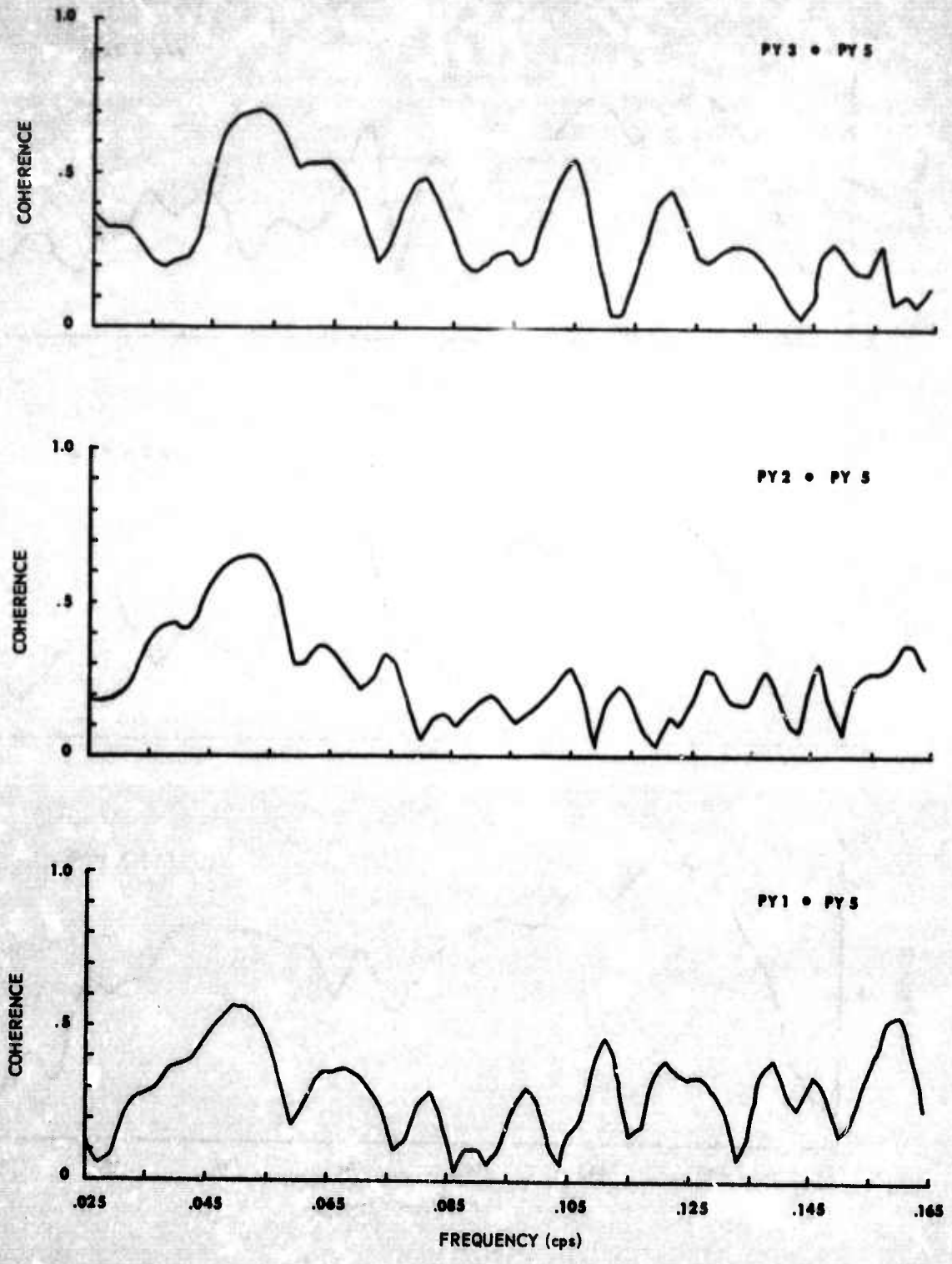

Figure 22. Coherence functions for data sample 1 for station separations greater than 25 kilometers

G 3159

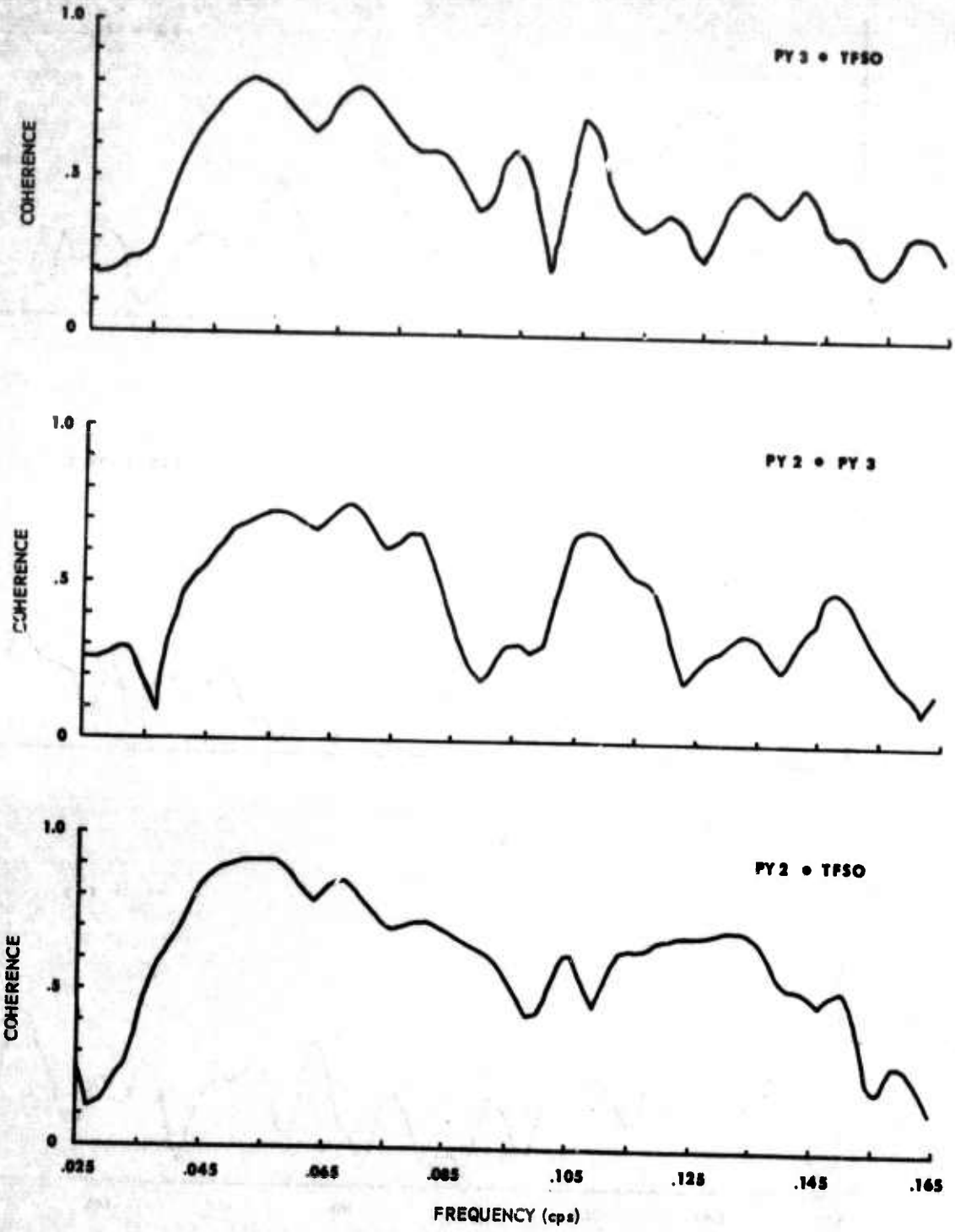

Figure 23. Coherence functions for data sample 2 for station separations less than 10 kilometers

G 3160

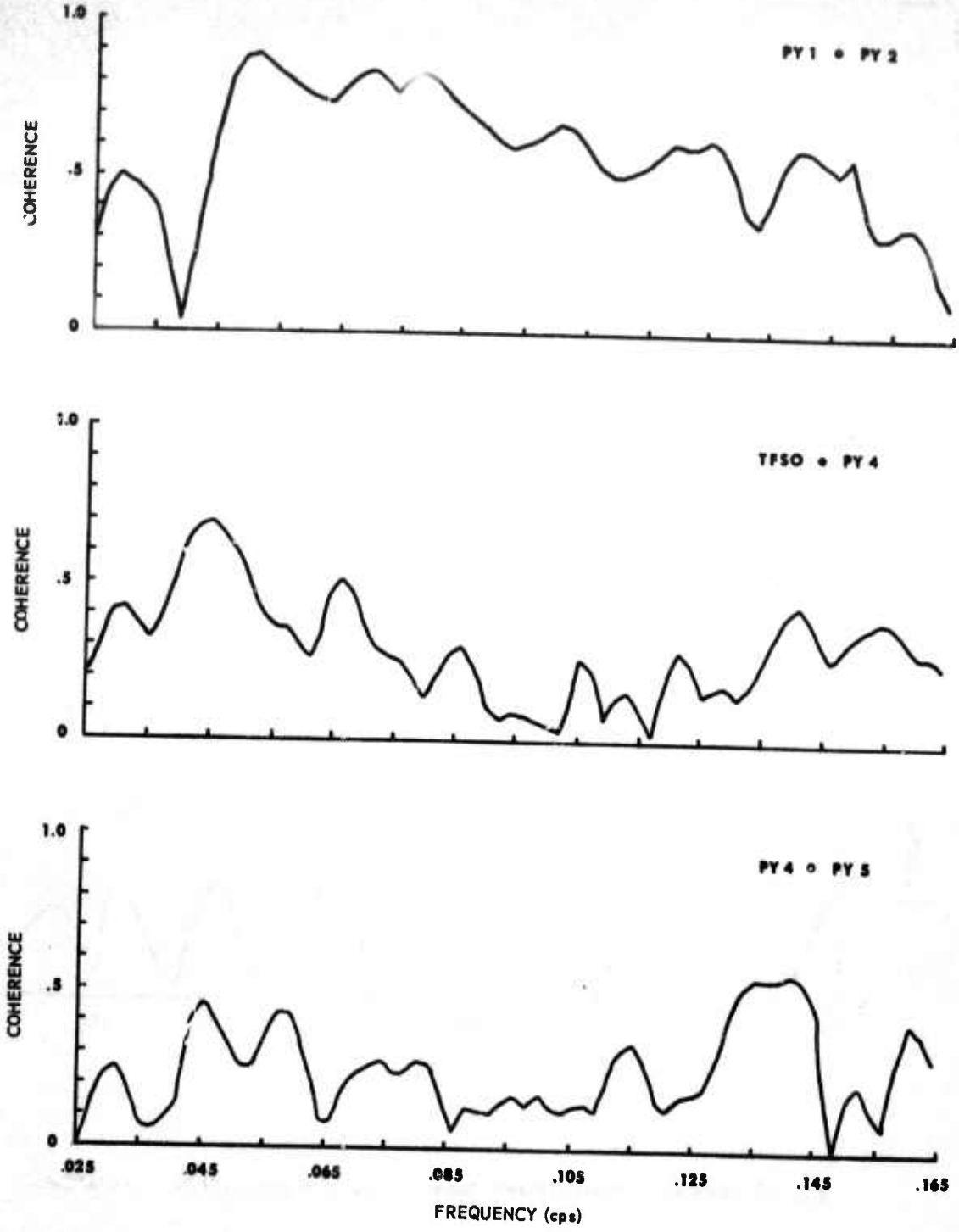

Figure 24. Coherence functions for data sample 2 for station separations of about 10 kilometers

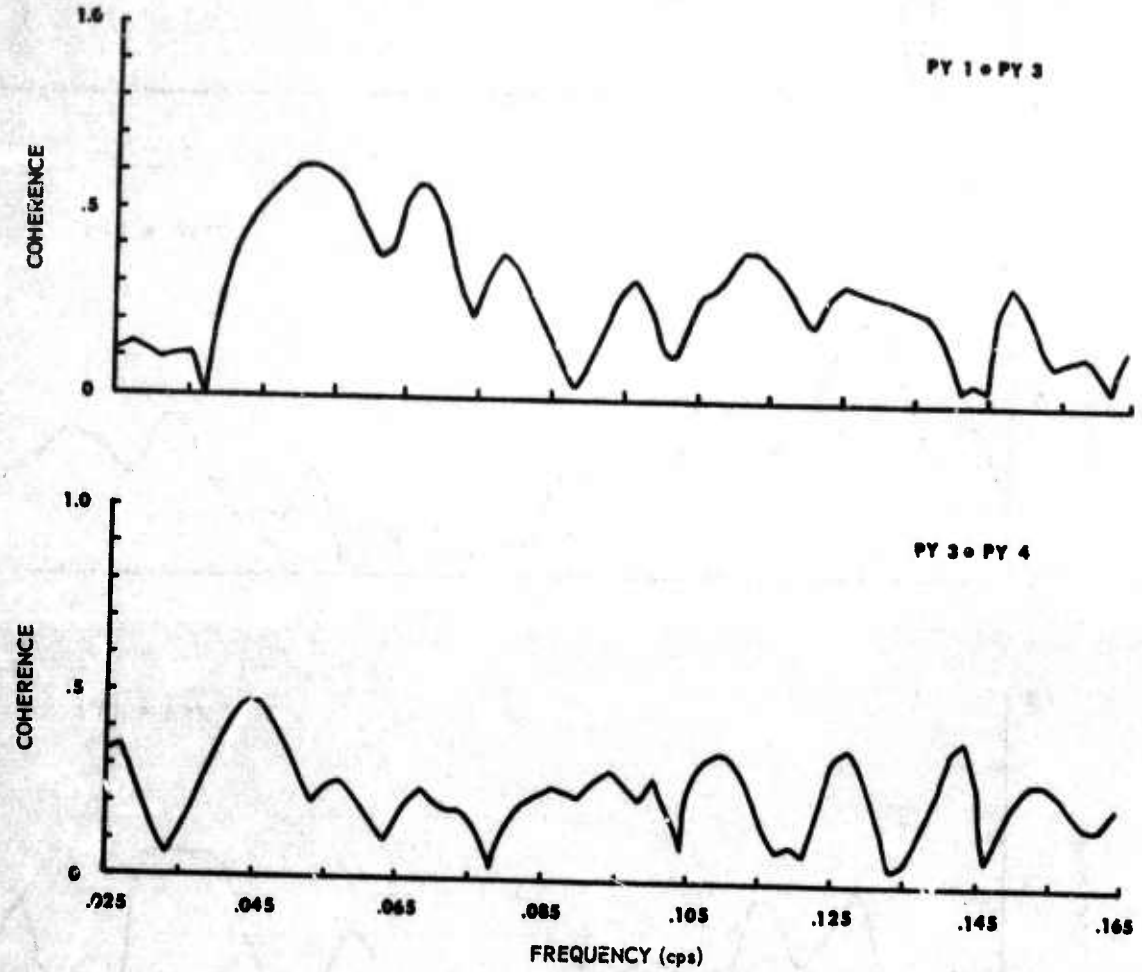

Figure 25. Coherence functions for data sample 2 for station separations of about 15 kilometers

G 3162

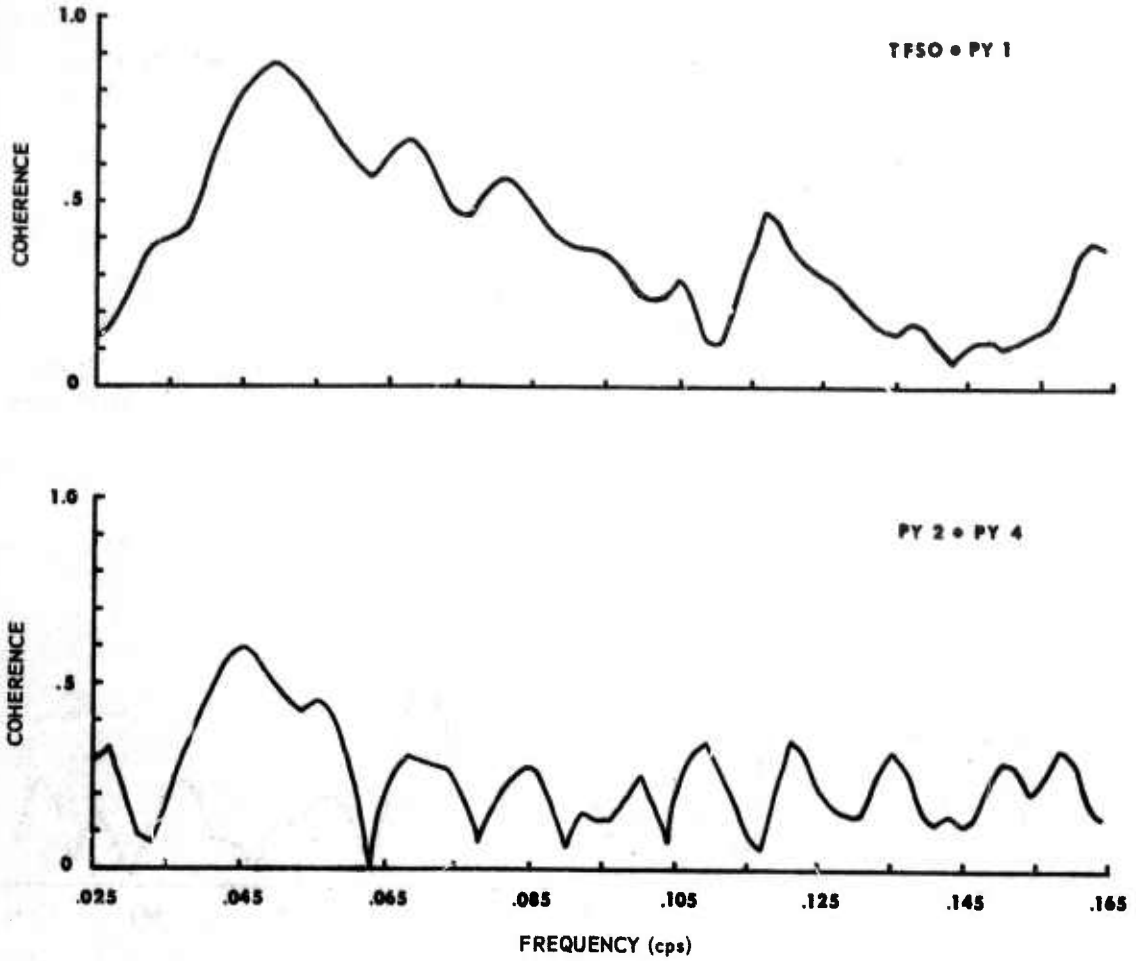

Figure 26. Coherence functions for data sample 2 for station separations of about 15.8 kilometers

G 3163

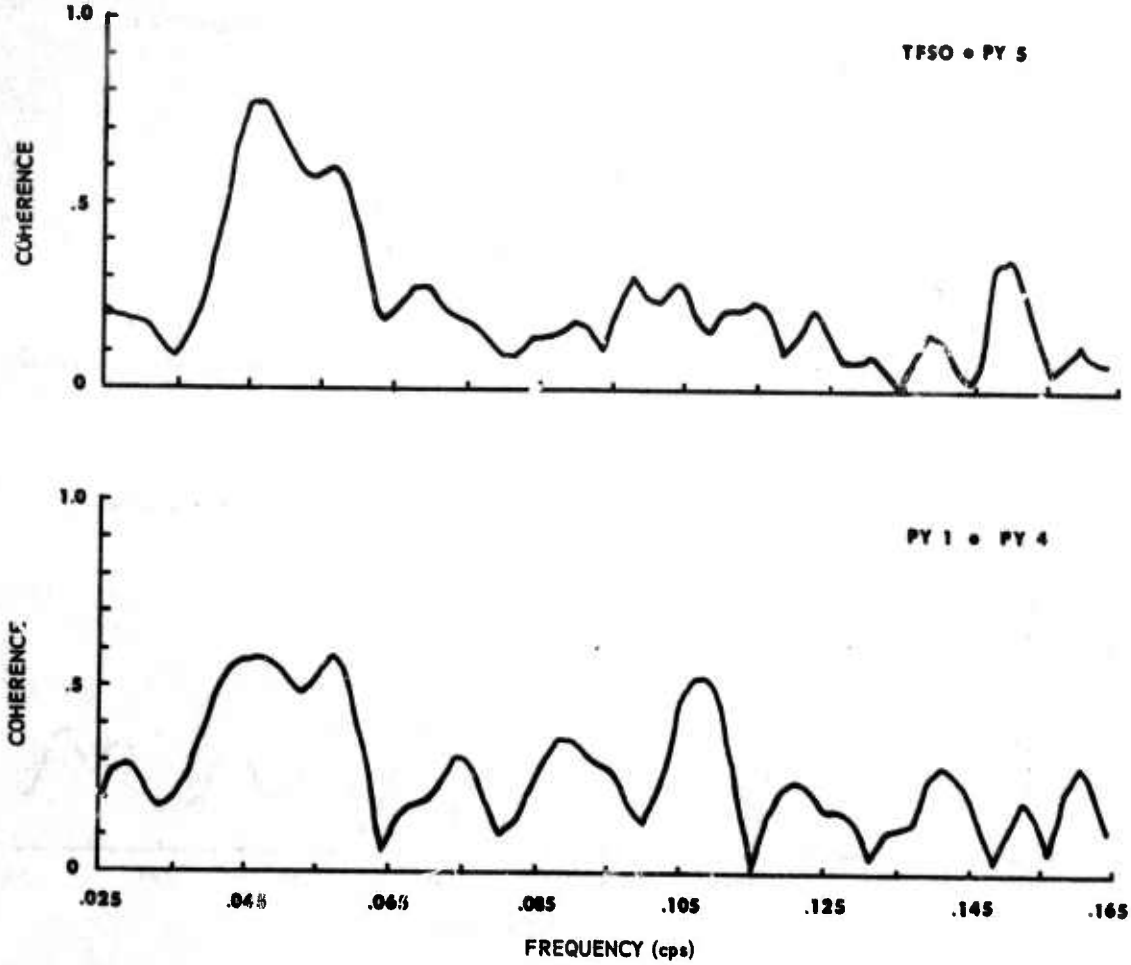

Figure 27. Coherence functions for data sample 2 for station separations of about 20 kilometers

G 3164

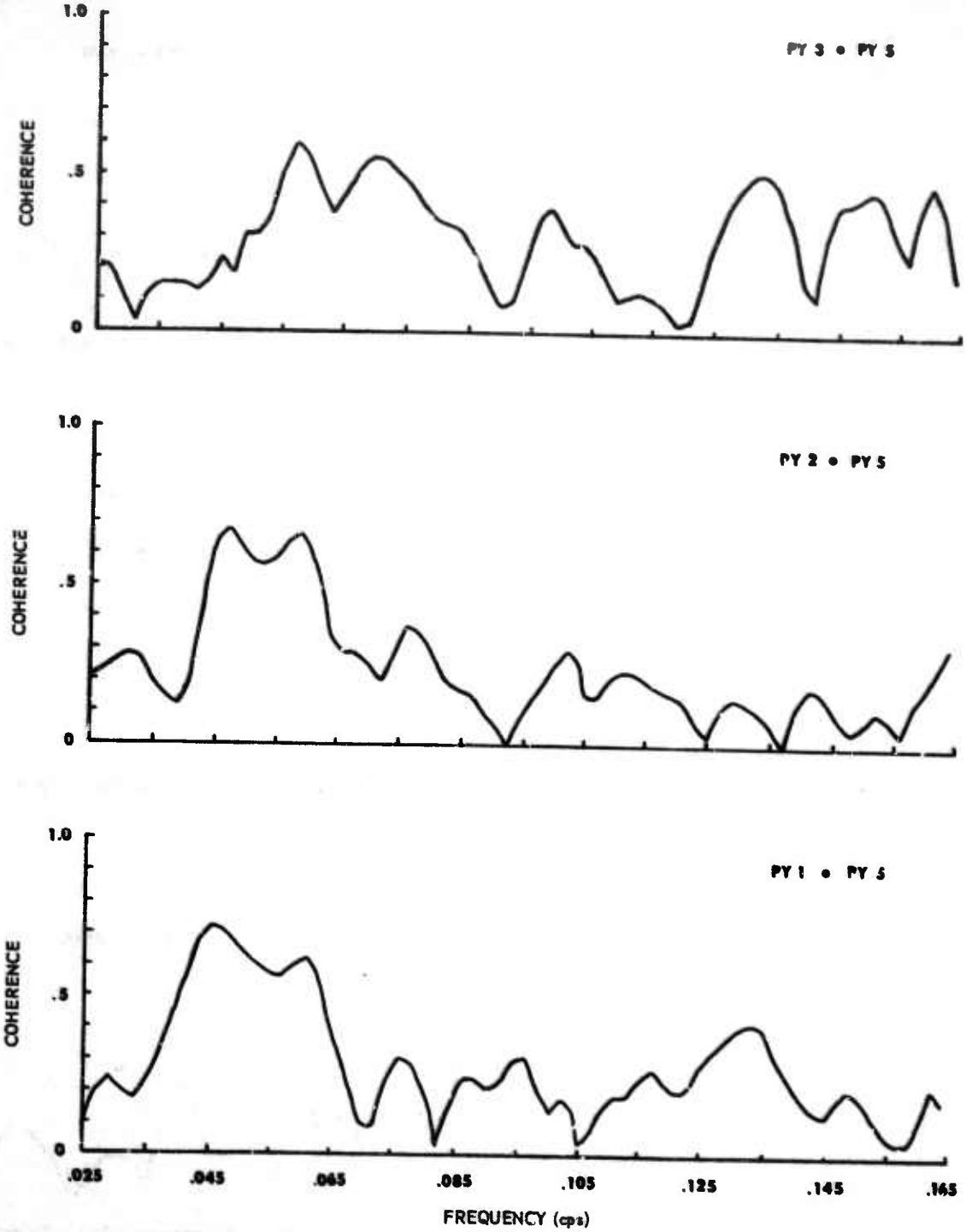

Figure 18. Coherence functions for data sample 2 for station separations greater than 25 kilometers

G 3165

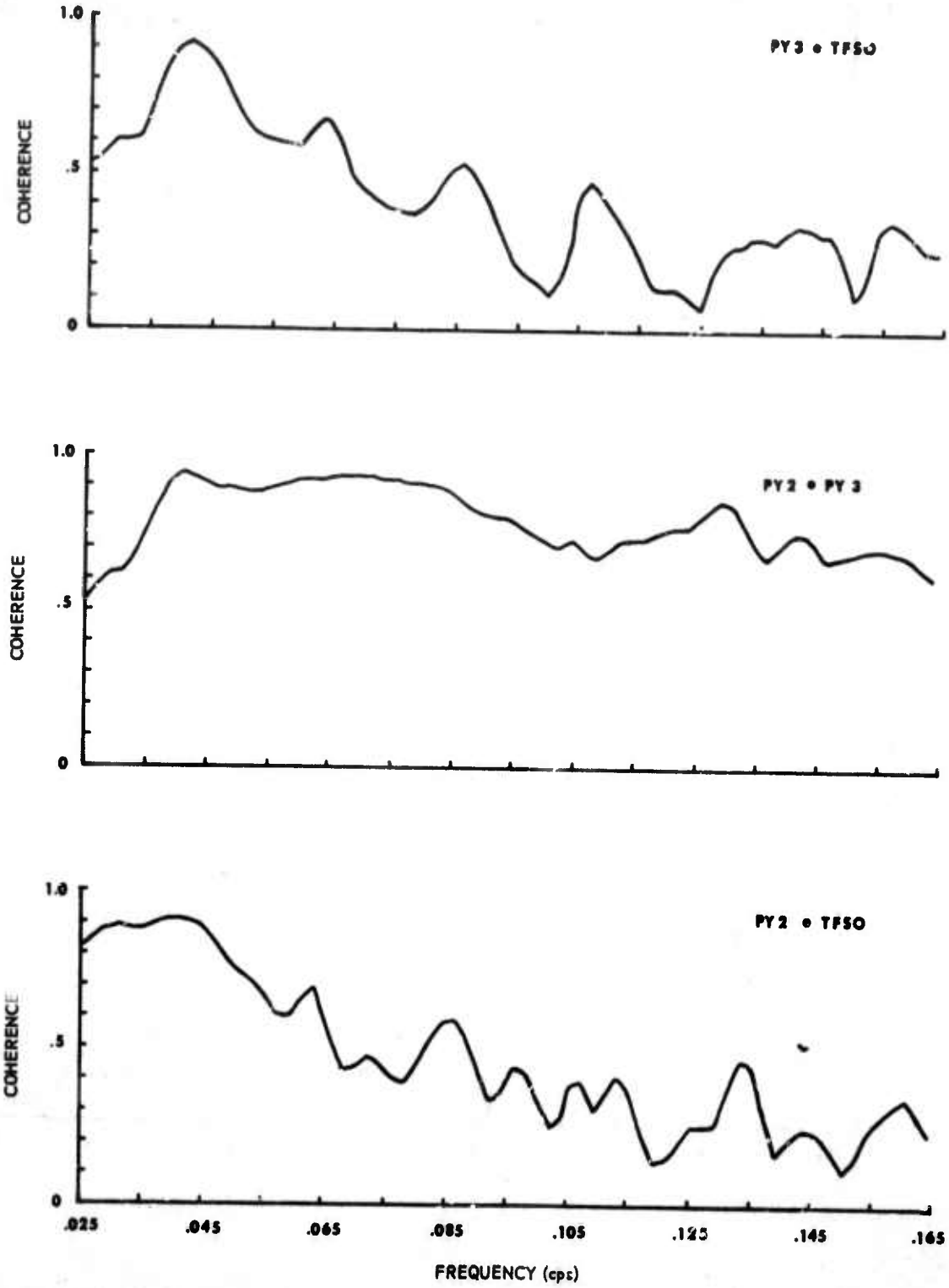

Figure 29. Coherence functions for data sample 3 for station separations less than 10 kilometers

G 3166

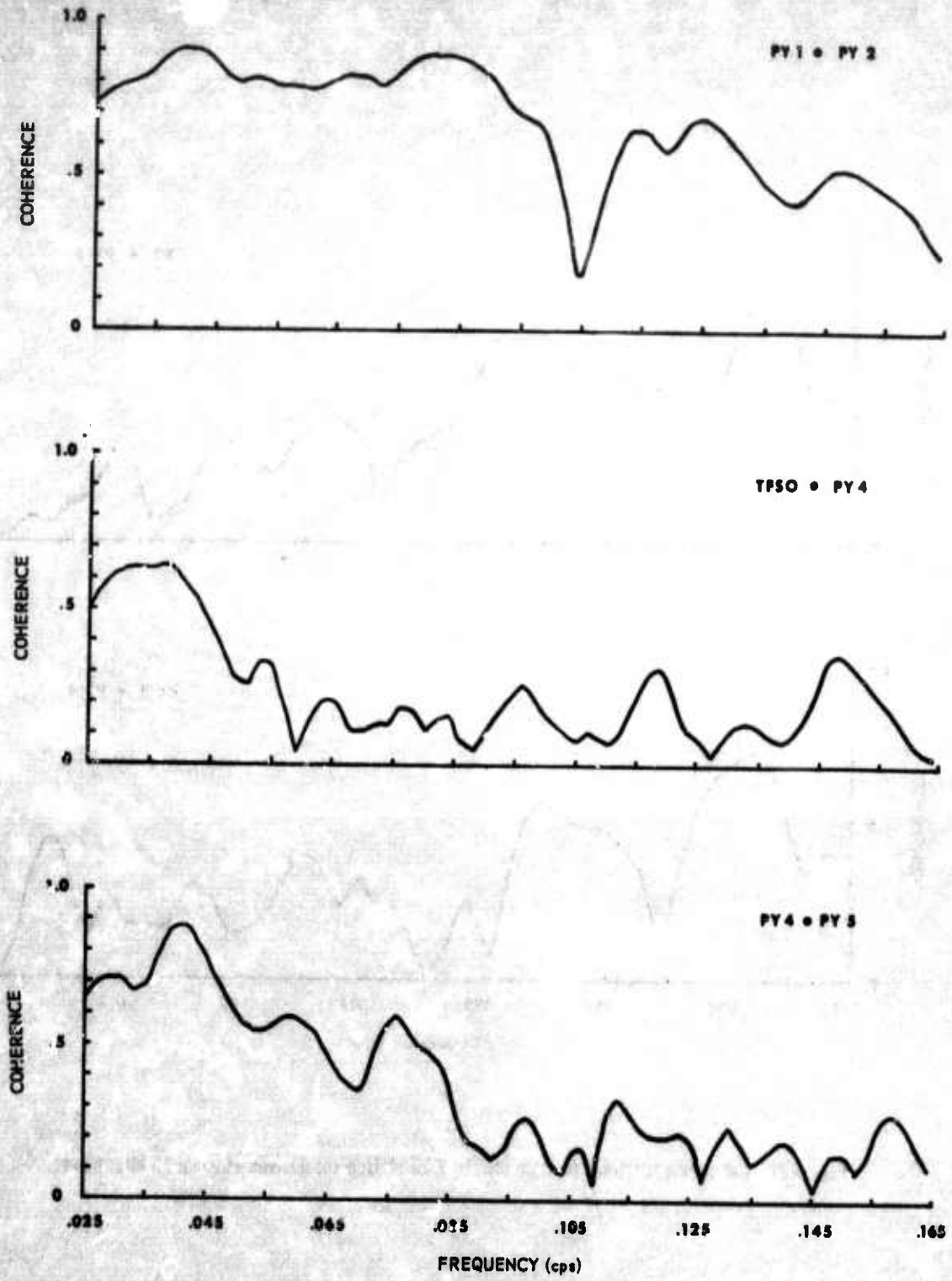

Figure 30. Coherence functions for data sample 3 for station separations of about 10 kilometers

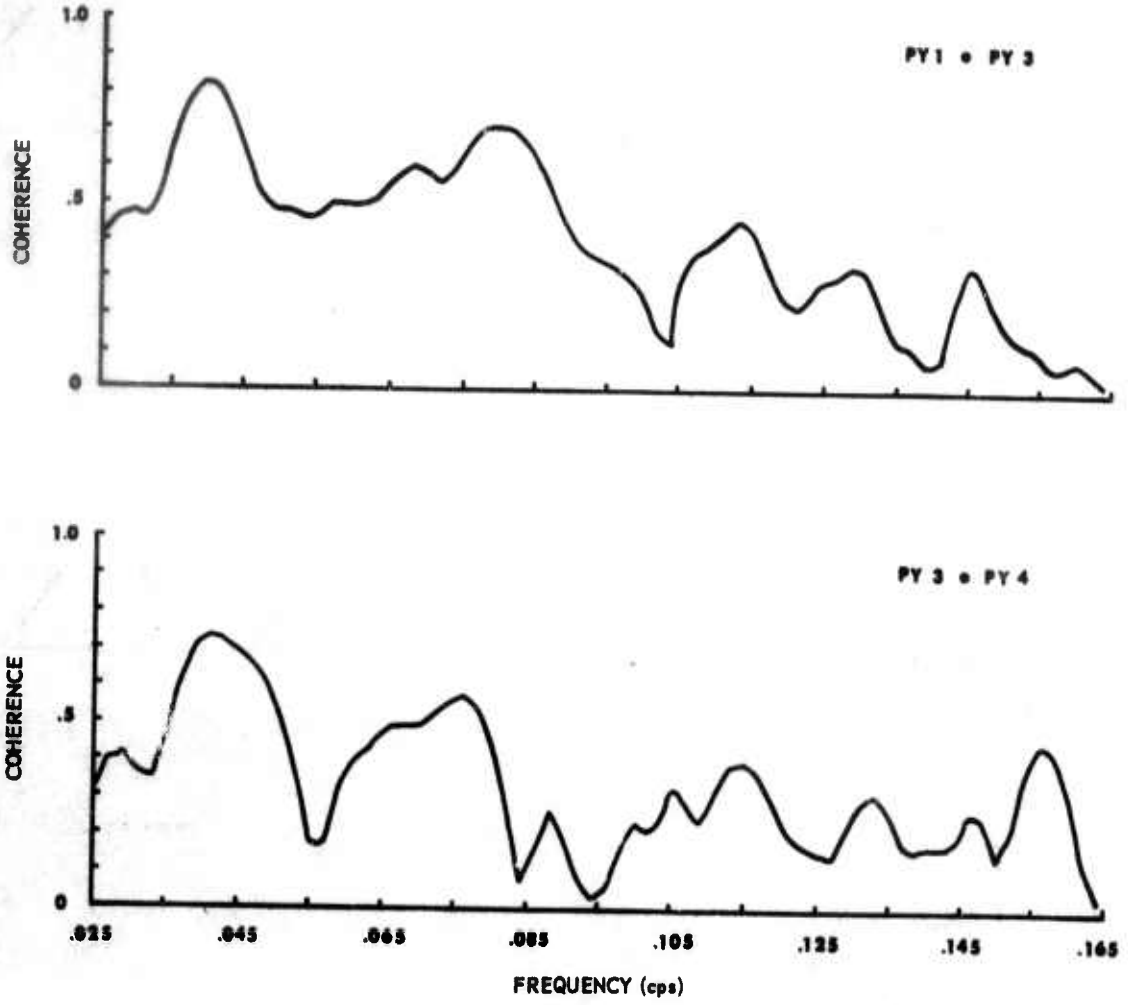

Figure 31. Coherence functions for data sample 3 for station separations of about 15 kilometers

G 3168

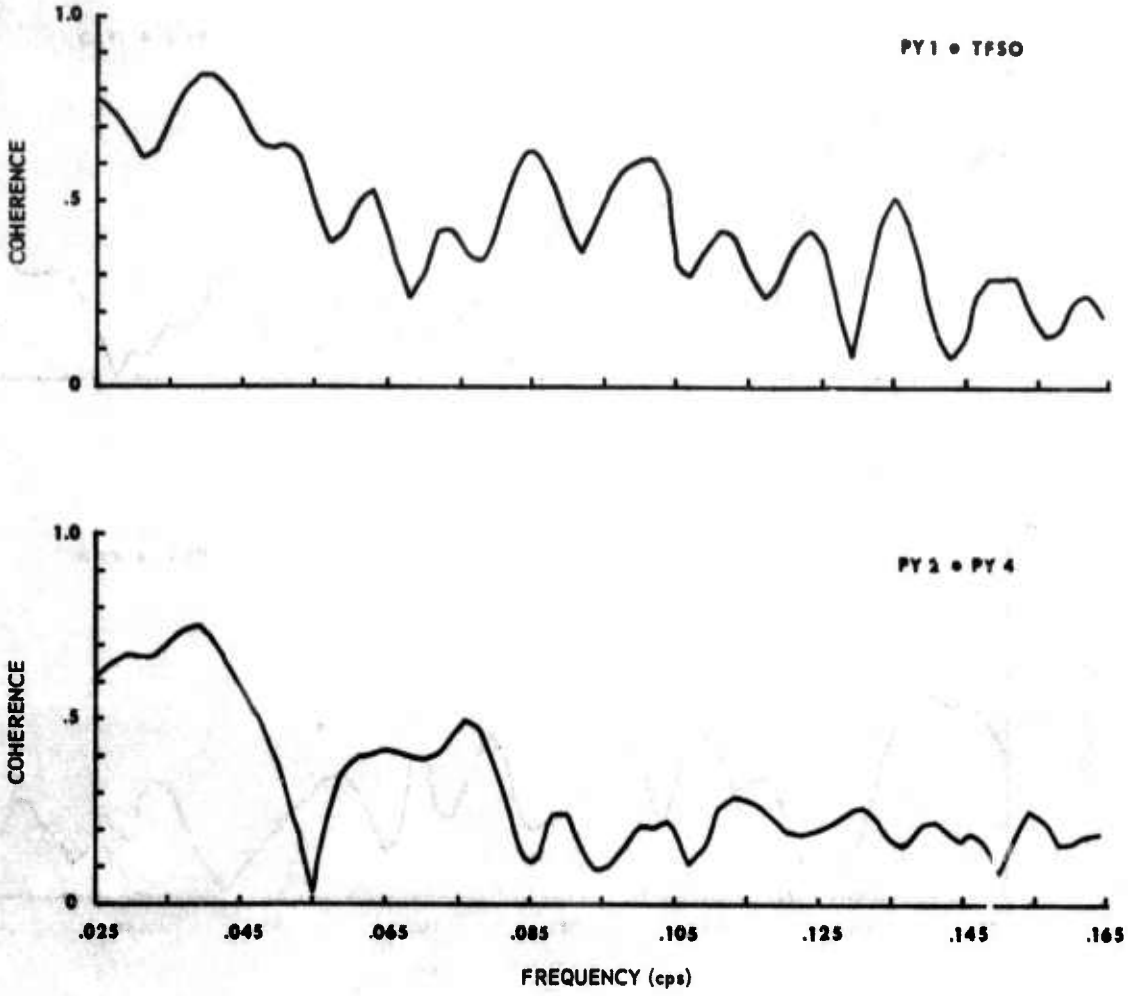

Figure 32. Coherence functions for data sample 3 for station separations of about 15.8 kilometers

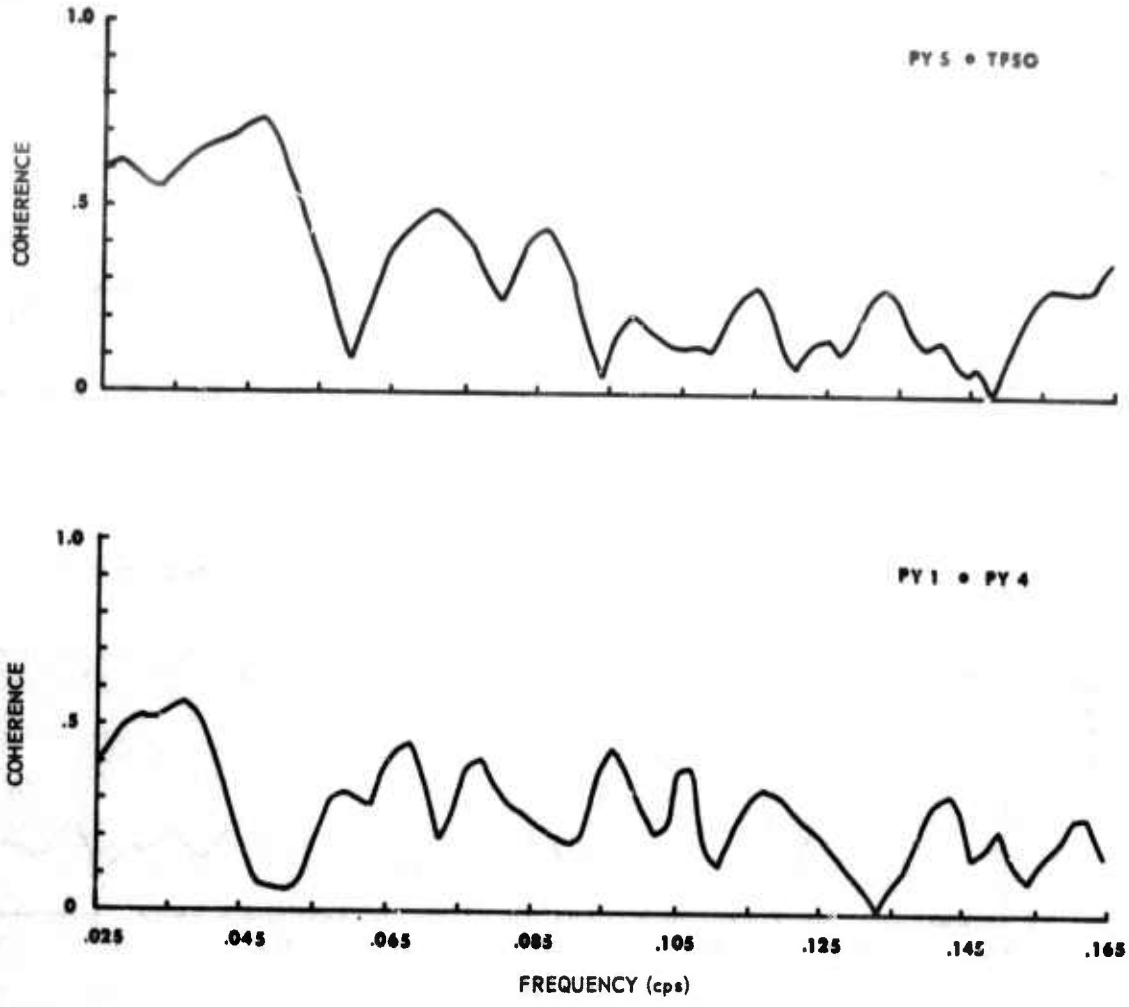

Figure 33. Coherence functions for data sample 3 for station separations of about 20 kilometers

G 3170

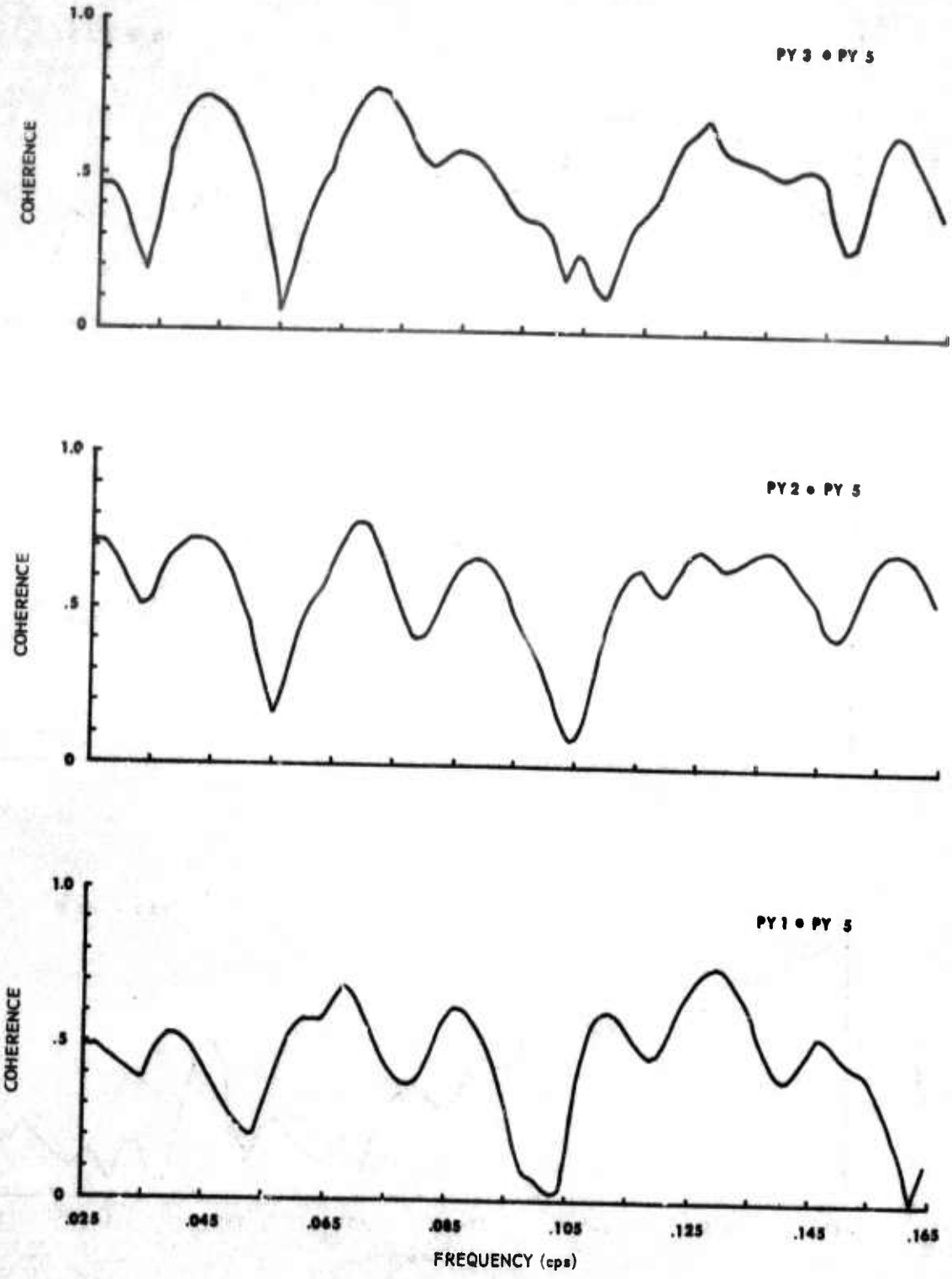

Figure 34. Coherence functions for data sample 3 for station separations greater than 25 kilometers

G 3171

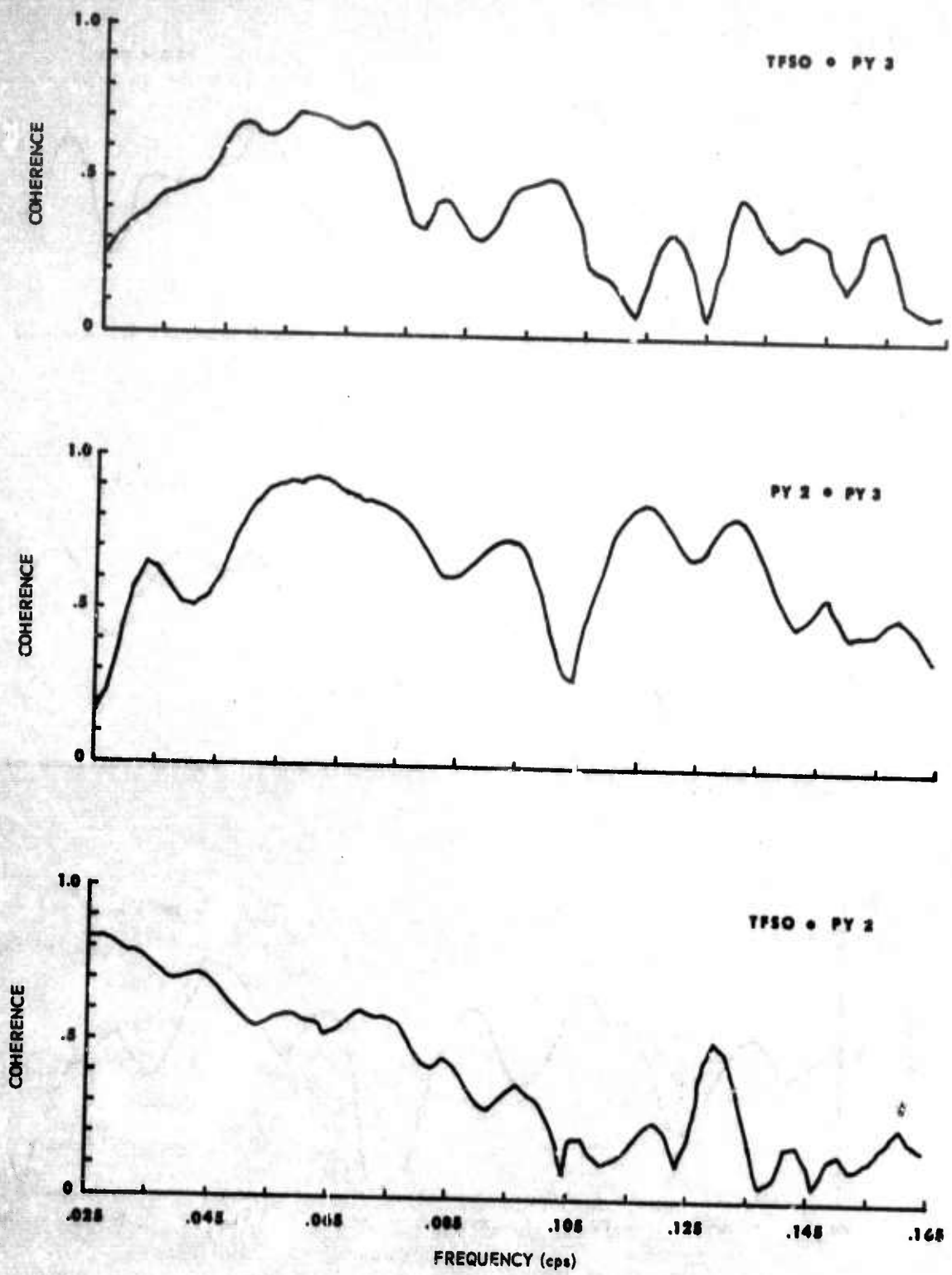

Figure 35. Coherence functions for data sample 4 for station separations less than 10 kilometers

G 3172

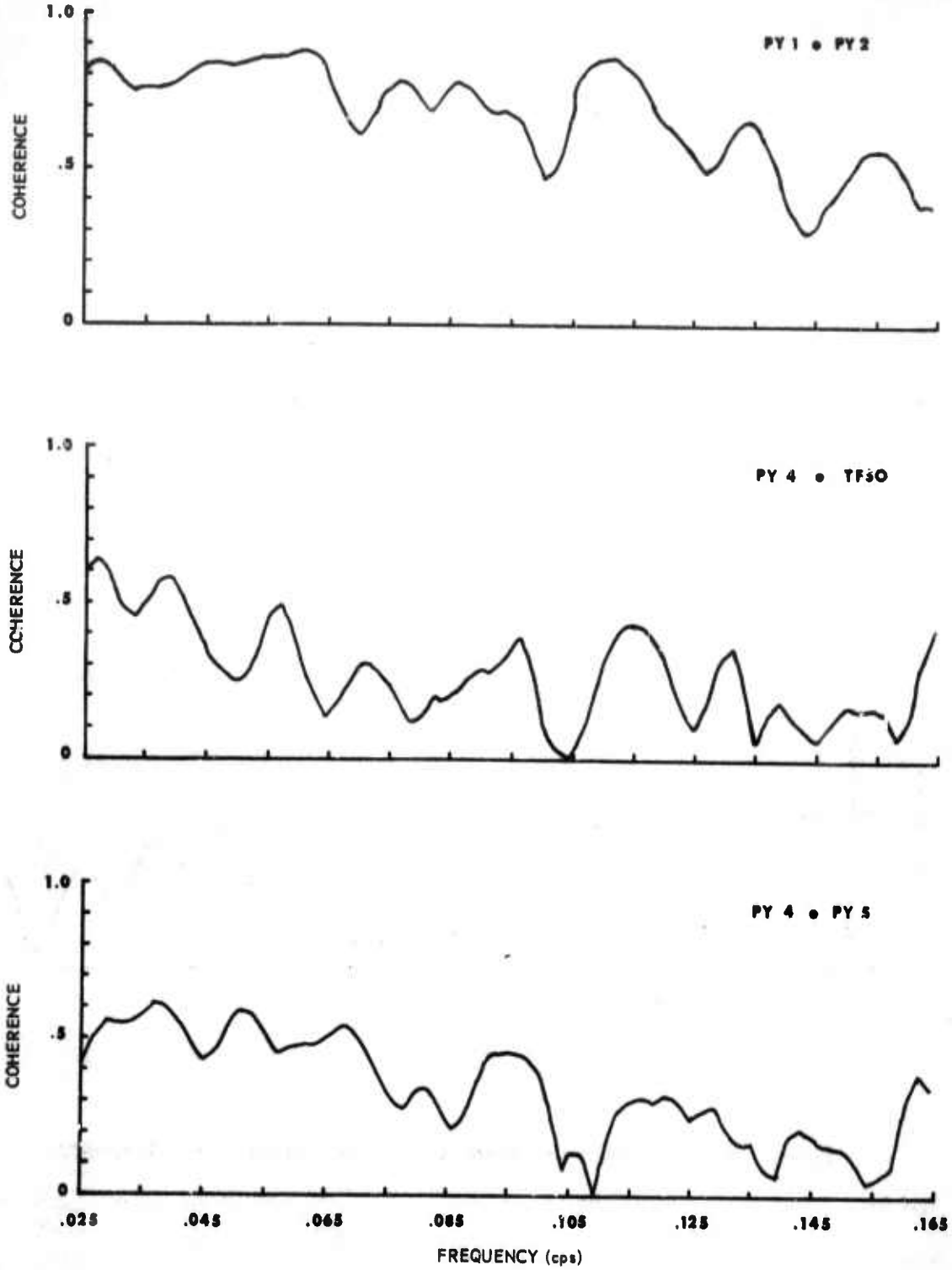

Figure 36. Coherence functions for data sample 4 for station separations of about 10 kilometers

G 3173

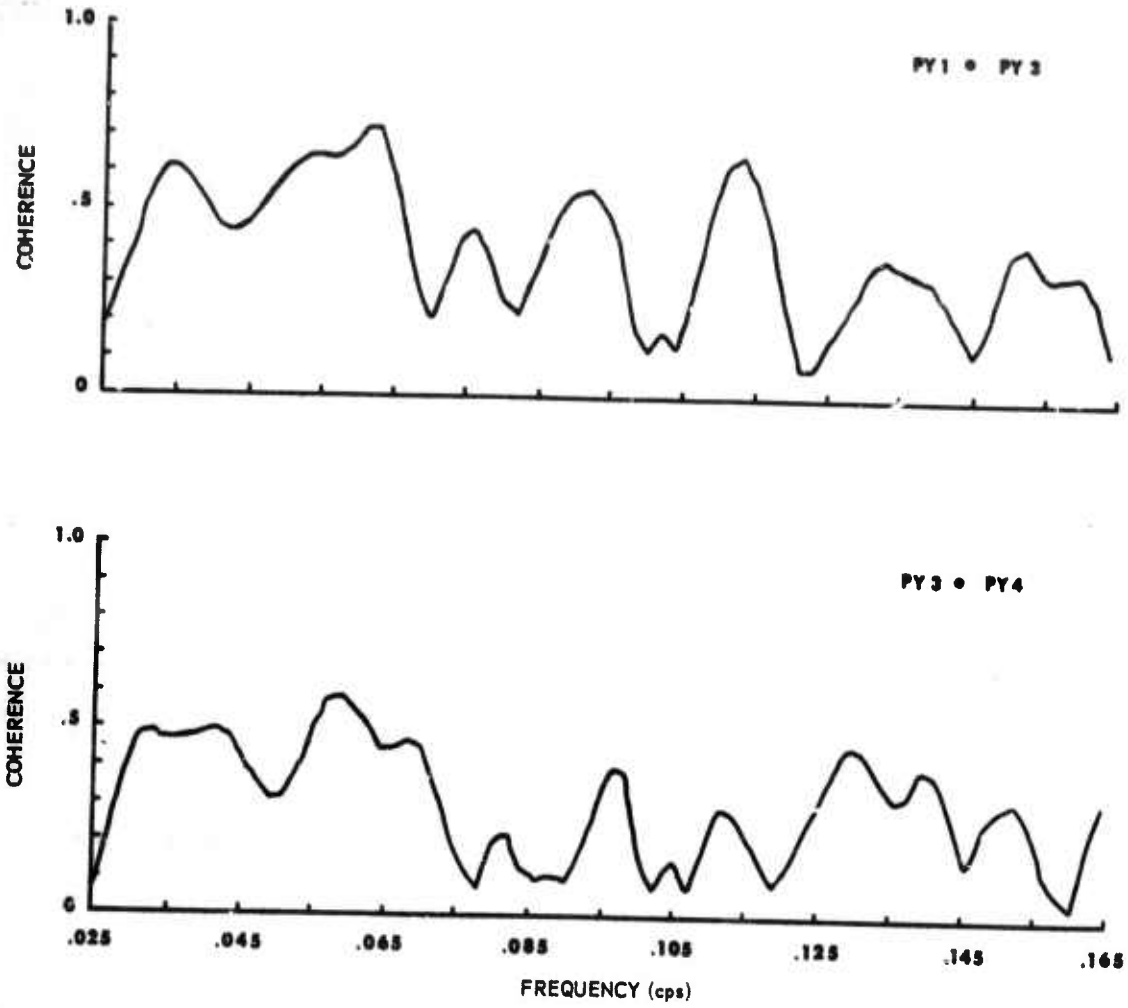

Figure 37. Coherence functions for data sample 4 for station separations of about 15 kilometers

G 3174

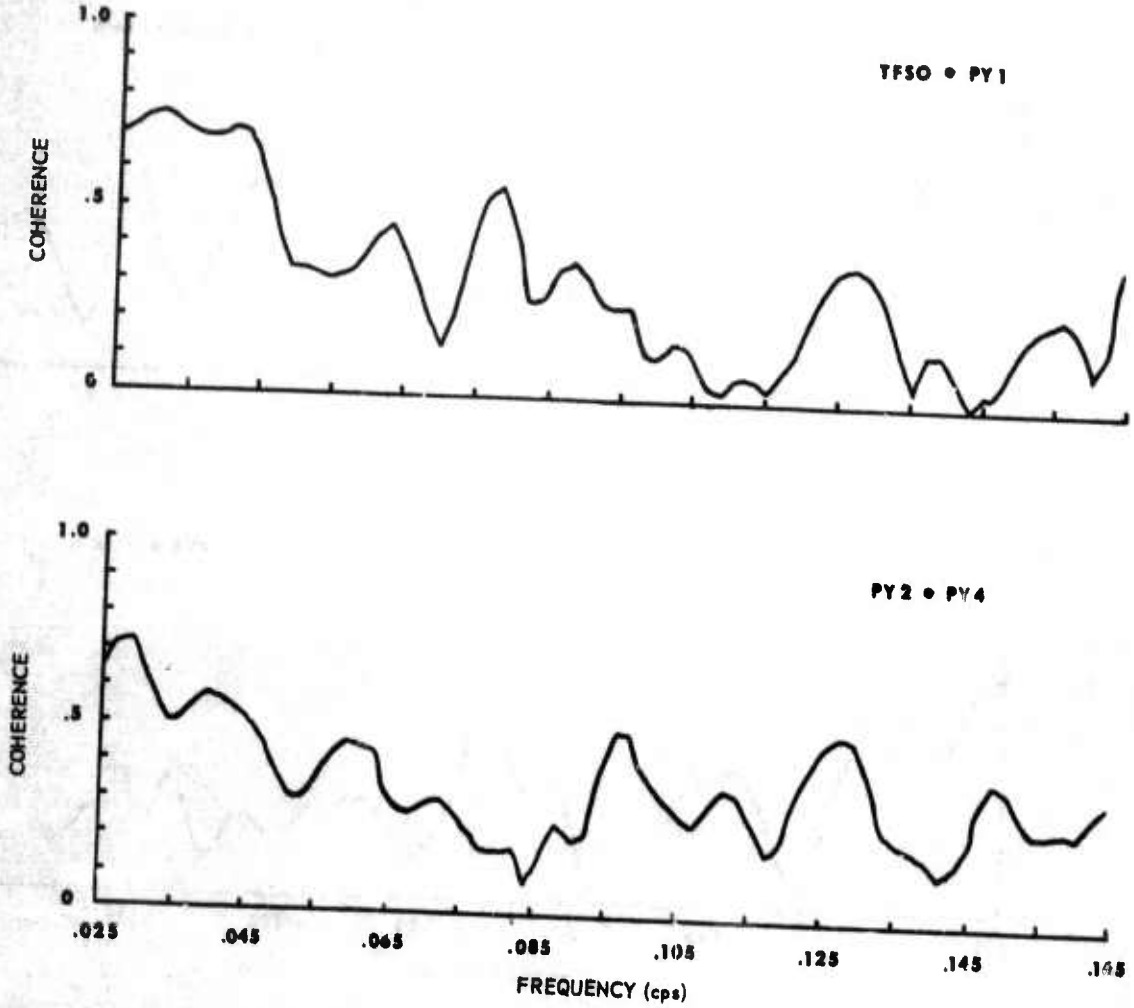

Figure 38. Coherence functions for data sample 4 for station separations of about 15.8 kilometers

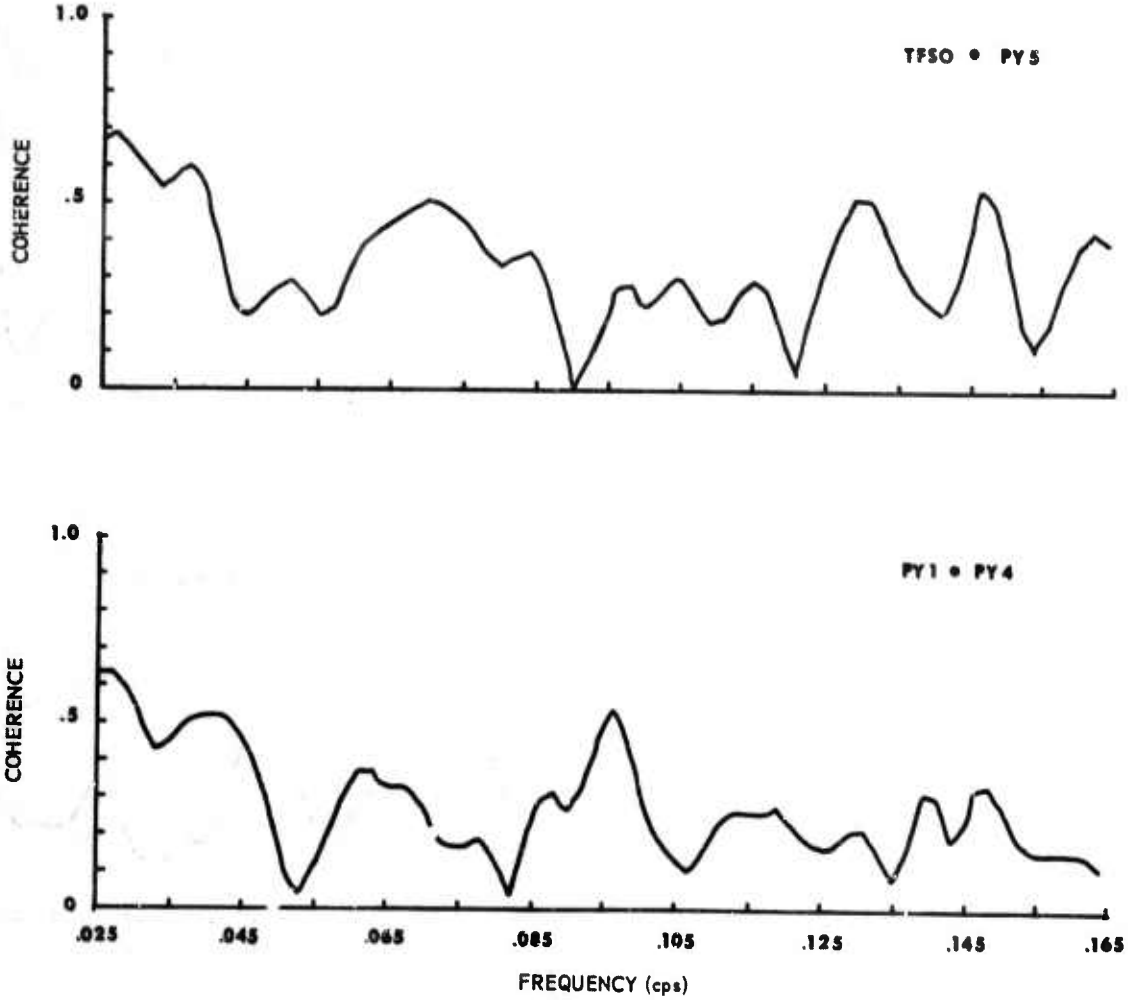

Figure 39. Coherence functions for data sample 4 for station separations of about 20 kilometers

G 3176

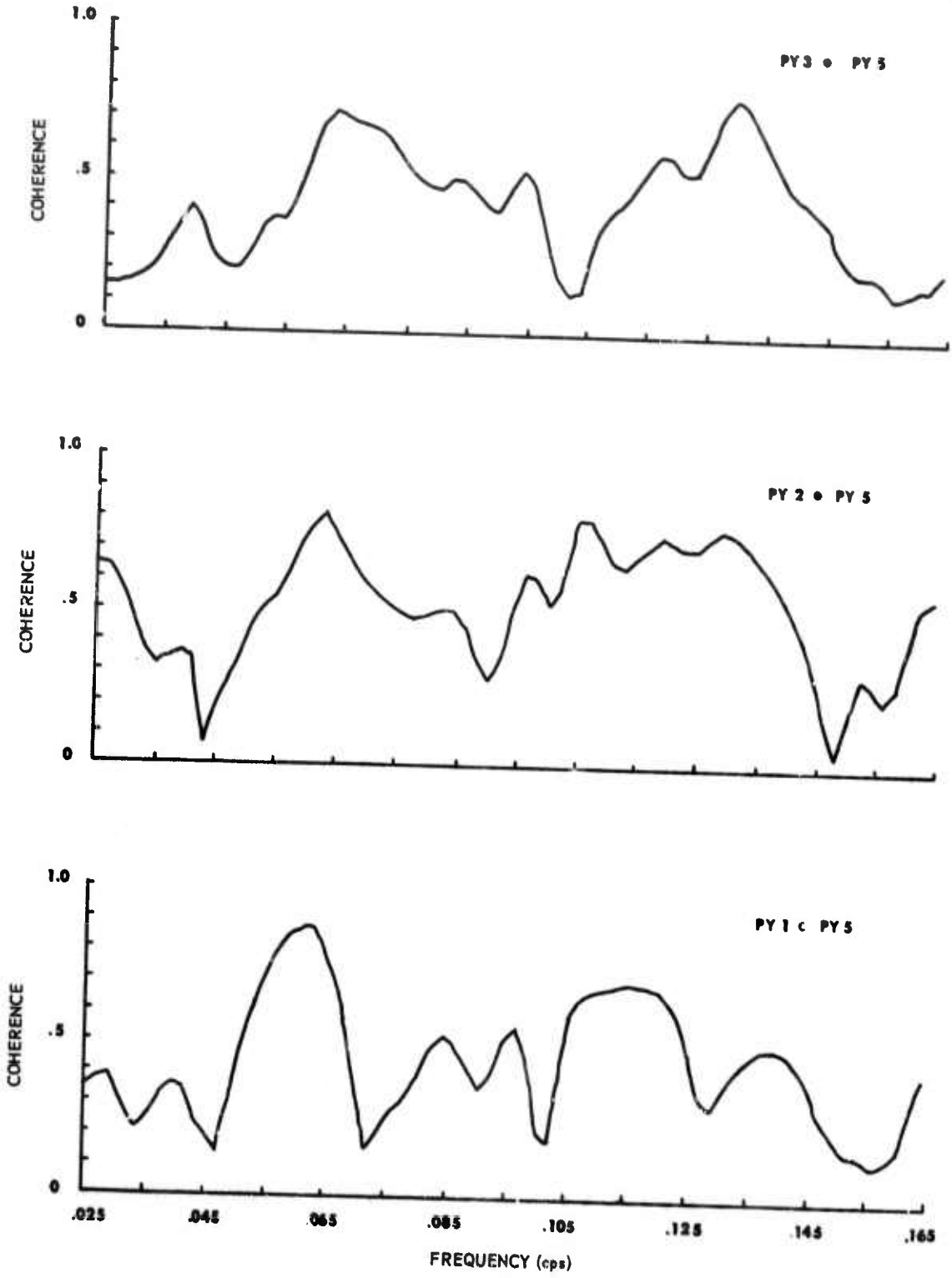

Figure 40. Coherence functions for data sample 4 for station separations greater than 25 kilometers

G 3177

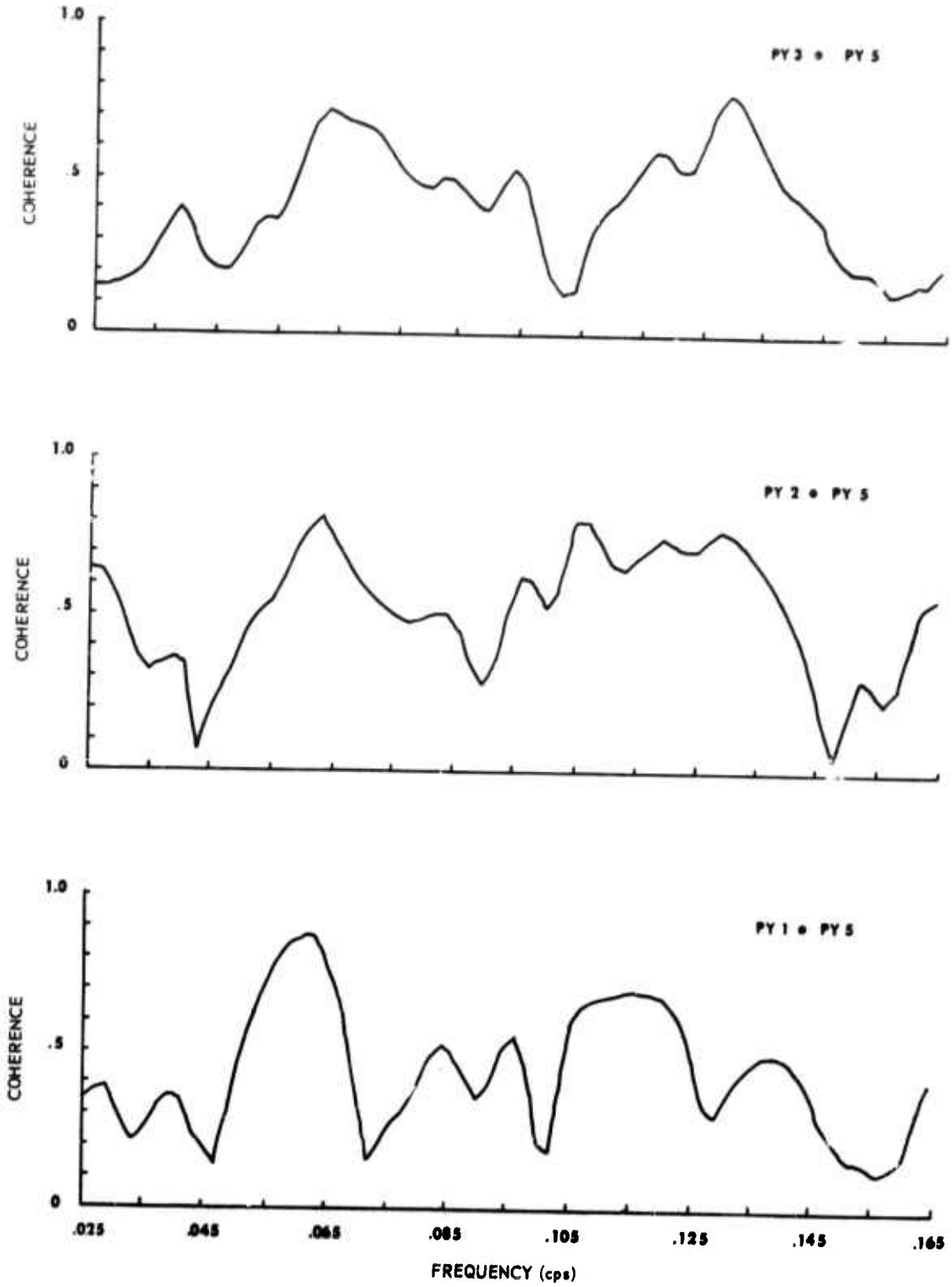

Figure 40. Coherence functions for data sample 4 for station separations greater than 25 kilometers

G 3177

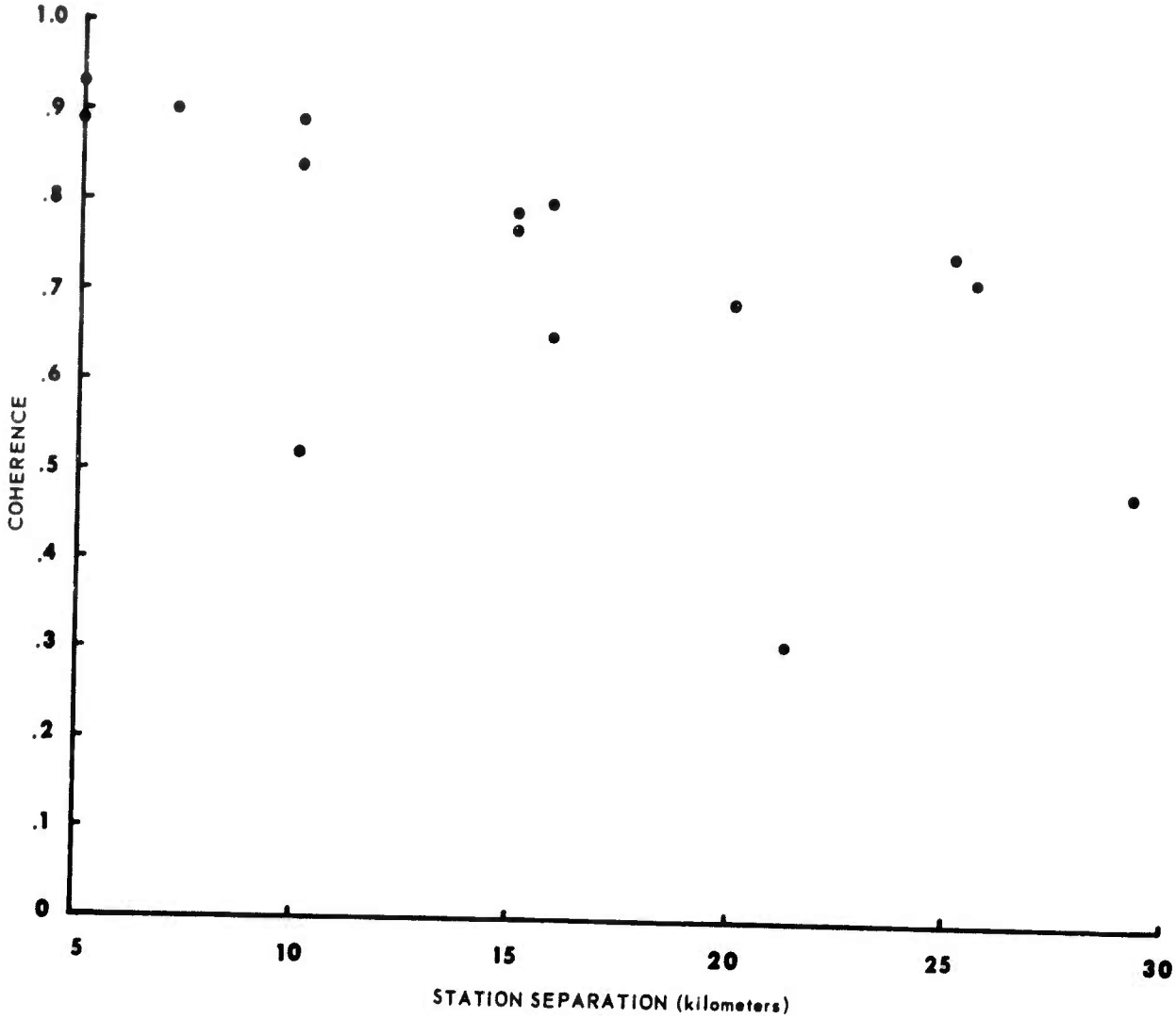

Figure 41. Coherence at 0.043 cps for data sample 3 as a function of distance between stations

G 3178

9.3 CONCLUSIONS

The overall level of the measured coherence was lower than expected, considering the size of the array and the wavelengths of the Rayleigh wave noise. The exact cause of the apparent degradation of the coherence is not clear. Possible causes of this are the existence of multiple noise sources and/or local geologic variations from site to site. There are not enough data available to determine the actual cause.

In summary, the following characteristics of coherence functions are evident:

a. The coherence functions are neither time nor space stationary.

b. The noise in the frequency band 0.04 to 0.082 cps shows high coherence for small station separations and the coherence in this band tends to decrease with increasing distance between stations.

c. The peak coherence usually occurs near the same frequency as the spectral peak in the frequency band 0.04 to 0.082 cps.

10. REFERENCES

Texas Instruments Inc., 1965, Array Research: Semiannual Technical Report No. 3, Contract AF 33(657)-12747, ARPA Order No. 104-60, Project Code 8100

Texas Instruments Inc., 1966, Array Research: Special Report No. 16, Initial analysis of long-period large aperture data recorded at the Tonto Forest Seismological Observatory in 1965, Contract AF 33(657)-12747, ARPA Order No. 104-60, Project Code 8100

Texas Instruments Inc., 1967a, Array Research: Special Report No. 23, Analysis of K-line wavenumber spectra from the TFSO long noise sample, Contract AF 33(657)-12747, ARPA Order No. 104-60, Project Code No. 8100

Texas Instruments Inc., 1967b, Continuation of basic research in crustal studies, Annual Report, Contract AF 49(638)-1588

Amos, D. E. and Koopmans, L. H., 1963, Tables of the distribution of the coefficient of coherence for stationary bivariate Gaussian processes: Sandia Corporation Monograph SCR483

UNCLASSIFIED

Security Classification

DOCUMENT CONTROL DATA - R & D

(Security classification of title, body of abstract and indexing annotation must be entered when the overall report is classified)

1. ORIGINATING ACTIVITY (Corporate author)
Teledyne Industries Incorporated
Geotech Division, 3401 Shiloh Road
Garland, Texas

2a. REPORT SECURITY CLASSIFICATION

2b. GROUP

3. REPORT TITLE
Analysis of TFSO Long-Period Noise Survey Data
Conducted under Project VT/7702

4. DESCRIPTIVE NOTES (Type of report and inclusive dates)
Special technical report

5. AUTHOR(S) (First name, middle initial, last name)
Dale S. Kelley

6. REPORT DATE
18 September 1967

7a. TOTAL NO. OF PAGES
56

7b. NO. OF REFS
5

8a. CONTRACT OR GRANT NO.
AF 33(657)-67-C-0091

b. PROJECT NO.
VELA T/7702

c. ARPA Order No. 624

d. ARPA Code No.

9a. ORIGINATOR'S REPORT NUMBER(S)
TR 67-54

9b. OTHER REPORT NO(S) (Any other numbers that may be assigned this report)

10. DISTRIBUTION STATEMENT
This document is subject to special export controls and each transmittal to foreign governments or foreign nationals may be made only with prior approval of the Chief of AFTAC

11. SUPPLEMENTARY NOTES

12. SPONSORING MILITARY ACTIVITY
Advanced Research Projects Agency
Nuclear Test Detection Office
Washington, D. C.

13. ABSTRACT

The installation and checkout of a medium aperture long-period array at Tonto Forest Seismological Observatory is described. Methods of data selection and preparation for processing are given. Power spectra and phase velocities of the noise are computed; comparison with previously reported results show basic agreement. Coherence functions show peaks at the same frequencies in which the noise power is concentrated. In the frequency band 0.04 to 0.082 cps, the peak coherence is greater than 0.8 for station separations less than 10 kilometers. The coherence tends to decrease with increasing distance between stations.

DD FORM 1 NOV 65 1473

UNCLASSIFIED

Security Classification

14 KEY WORDS	LINK A		LINK B		LINK C	
	ROLE	WT	ROLE	WT	ROLE	WT
Long-period noise study Coherency of long-period noise as a function of distance Power spectra of long-period noise Phase velocity of long-period noise 0.04 to 0.082 cps long-period noise Vault installation for LRSM portable systems Computation of coherence functions						